

March 2017

SMA wire actuator in a morphing wing

# INTERNSHIP REPORT

Joran Driesen, s1201557

**Faculty of Engineering Technology**

Supervisor Twente University:  
Richard Loendersloot

Supervisors ITA:  
Luiz Carlos Sandoval Góes  
Osmar De Sousa Santos



UNIVERSITY OF TWENTE.



# Preface

I searched for an internship all around the world and ended up in Brazil. I want to thank Richard Loendersloot, because it was his connection with Luiz Goes that made this internship possible in the first place. I want to thank Luiz Goes for making the arrangements, and getting me an entrance badge within the first two days. Even though he is a very busy man, he always had time to talk to me. He put me in contact with a lot of people and because of that I got to do a project that I really liked with Osmar Santos. Osmar helped me a lot, both with the project and life in Brazil. I really enjoyed our conversations about life in Brazil, Europe, politics and physics. I think I can say we became friends. I have never met a guy who was so interested in doing and understanding all things in life. Law, politics, teaching, diplomacy, physics, engineering, foreign languages, he wants to do it all!

The application of SMA wire in morphing wings was very interesting to work with. Morphing wings are cutting edge technology and using SMA wire to achieve this is something that I believe is only done here in Brazil. I am very practical orientated and I enjoyed figuring out the things that come with prototype work. I hope I made a useful contribution to the aeronautical world. I wrote a paper about this work and it has been accepted by the AIAA SciTech conference of January 2018!

I really had a good time in Brazil. The country is big and beautiful, the people are very friendly and there is so much to see and do. I liked it so much I am returning for a year to do a double degree at ITA!



# Summary

The design of an air foil is usually a compromise between the requirements of different flight conditions. Commercial airliners usually spend most of their time cruising, and therefore the air foil is optimized for that condition. UAV drones however have a different mission profile, spending time on cruising, loitering, ascending and descending. A morphing wing that can change its air foil to optimize the efficiency during the entire mission profile will be highly beneficial. Another possibility is to use the morphing capabilities of the wing as actuation. Twisting of the wing can act as an aileron and a wing bend over its profile can act as a flap. This will eliminate the need for separate control surfaces on the wing. A morphing wing will change its surface smoothly, instead of the disruptive change of current actuators. This will make the wing smoother, quieter and more efficient. The research described in this report will expand upon earlier research done at ITA by Campos de Almeida, and tries to see if it is possible to create a functioning morphing wing that can bend both upwards and downwards, using shape memory alloy (SMA) wire. SMA is a material that is able to elongate up to 8% and recover its original shape when heated (Lagoudas, 2008). The wire will be attached inside the wing in elongated form. When heated it will shrink to its normal length, bending the wing. A morphing wing was designed and constructed, using 7 3d-printed PLA ribs with a NACA0012 profile. These ribs were connected with rods to create a wing frame. 12 SMA wires were attached to the frame. See figure 1 and 2.



**Figure 1:** Drawing of one of the ribs with one SMA wire attached. The antagonistic wire is attached in the same way, but mirrored over the horizontal symmetry axis and slightly off-set in depth direction, to prevent contact with the opposing wire.

The SMA wires were attached to electrical wires and the frame was covered with

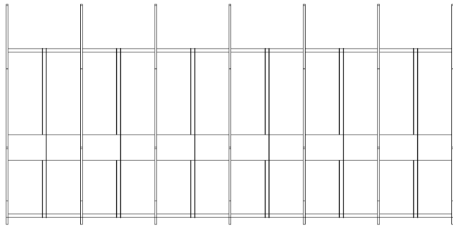


**Figure 2:** Top down view of wing frame



**Figure 3:** Finished wing

model wood sheets to create a smooth surface. A 12 mm diameter rod was attached to the wing in order to clamp it in the wind tunnel. The finished wing can be seen in figure 3.

The wing was placed inside a subsonic wind tunnel at Professor Feng Laboratory that belongs to Aeronautic Engineering Division from Instituto Tecnológico de Aeronáutica (ITA). The wind tunnel has a 457 mm by 457 mm cross-section and is 1200 mm in length. The wind tunnel is outfitted with a force moment balance and a pressure sensor. The wing was tested multiple times in three configurations: unactuated, actuated upwards and downwards, see figure 4. The lift coefficient was plotted against the angle of attack. The results can be found in figure 5. The symbols show the error margin caused by the noise in the signal. It can be seen that the morphing states of the wing shift the  $C_l$  graph, acting like a flap.

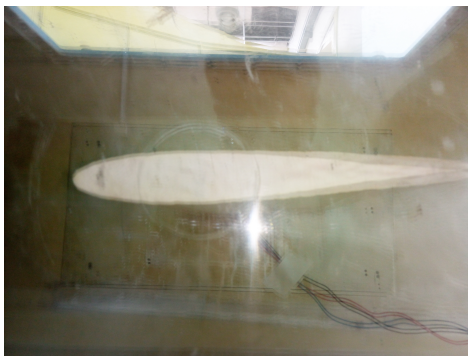


**Figure 4:** Overlay of two pictures, comparing the two extreme positions of the morphing wing.

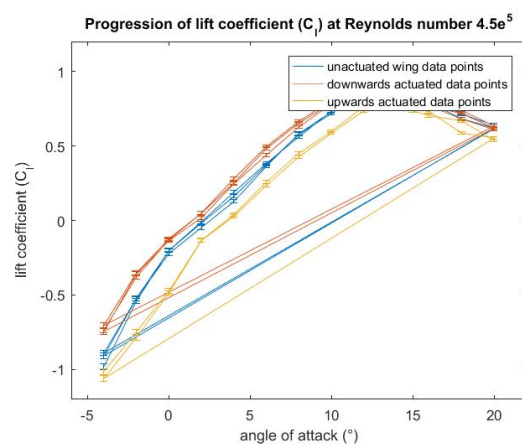


**Figure 5:** Lift coefficient function for the three states of the morphing wing.

This research set out to prove that SMA wire can be used as an actuator and in that it succeeded. The tests in the wind tunnel show that even with the 2-mm deflec-

tion caused by the SMA wire, the characteristics of the wing change considerably. This proves that SMA is a feasible actuator in a morphing wing. This opens the way for new research into extending the range of motion of the wing and optimizing the morphed air foil shape. Other forms of morphing, like twisting and sweeping can be implemented too. When a control system is made for the actuation of the wires, a prototype wing could be fabricated and tested on a RC plane.



# Contents

<b>Preface</b>	<b>iii</b>
<b>Summary</b>	<b>v</b>
<b>List of acronyms</b>	<b>xi</b>
<b>1 Introduction</b>	<b>1</b>
<b>2 Background study</b>	<b>3</b>
2.1 Shape Memory Alloy . . . . .	3
2.1.1 SME cycle . . . . .	3
2.1.2 SMA training . . . . .	5
2.1.3 SMA actuator . . . . .	6
2.2 Morphing Wings . . . . .	7
<b>3 Design</b>	<b>11</b>
3.1 Functions and demands . . . . .	11
3.2 Concepts . . . . .	12
3.2.1 Concept Tubo Dobradiça . . . . .	12
3.2.2 Outwire . . . . .	12
3.2.3 Inwire . . . . .	13
3.2.4 Selection . . . . .	14
3.3 Refining ribs . . . . .	14
3.3.1 Wire placement . . . . .	15
3.3.2 Test set-up . . . . .	15
3.3.3 Results . . . . .	16
3.4 Framework . . . . .	17
3.5 Final Design . . . . .	17
<b>4 Fabrication</b>	<b>21</b>

---

<b>5</b>	<b>Testing</b>	<b>29</b>
5.1	Table testing . . . . .	29
5.2	Wind tunnel testing . . . . .	30
5.2.1	Description of equipment . . . . .	30
5.2.2	Calibration . . . . .	32
5.2.3	Testing . . . . .	34
<b>6</b>	<b>Results and Discussion</b>	<b>37</b>
6.1	Table test results . . . . .	37
6.1.1	Rib deflection mechanism . . . . .	40
6.2	Surface deflection . . . . .	41
6.3	Wind tunnel test results . . . . .	43
<b>7</b>	<b>Conclusions and Recommendations</b>	<b>47</b>
7.1	Conclusions . . . . .	47
7.2	Recommendations . . . . .	47
	<b>References</b>	<b>49</b>
	<b>Appendices</b>	

# List of acronyms

<b>SMA</b>	Shape Memory Alloy
<b>SME</b>	Shape Memory Effect
<b>LAp</b>	Laboratório de Aplicações
<b>MAS</b>	Morphing Aircraft System
<b>DOF</b>	Degree of Freedom



## Introduction

Air planes and drones rely on flaps actuated by bulky hydraulics or servos to steer. These control surfaces often have gaps between them and the wing and their sudden increase in angle results in an increase in drag and noise [1]. There is a field of research that seeks to remedy this problem [2]. Recently, studies have looked to morphing wings for a solution [3] [2] [4] [5] [6] [7] [8] [9] [10]. These wings can twist and bend their surface, making current ailerons, flaps, rudder and elevators obsolete.

The technology to make flexible wings is something that has existed for a long time. The plane made by the Wright brothers relied on morphing wings to steer. The lightweight wood with linen structure of the wing had ropes attached to its ends. These ropes were pulled, causing the wings to twist and the plane to pitch or roll [18]. The challenge lies with balancing stiffness and flexibility. The wing need to be stiff enough to withstand the aero dynamical load without deforming too much. But still be flexible enough to be actuated easily. Another problem is the actuator itself. Current control surface actuators are bulky and are placed under the wing, encapsulated in anti-shock bodies in order to minimize the increase in drag. A morphing wing would need a lot of actuators in order to smoothly change the shape of the whole wing. This feat is impossible using servos.

A solution for this problem is Shape Memory Alloy (SMA) wire. This wire has the ability to contract around 8% when subjected to heat [11]. This process is reversible, making it ideal for deforming a wing. This wire can be placed inside the wing along its length. By controlling the temperature of each wire, the wing can either be bent or twisted [12]. The process is too slow for application in flaps and ailerons. In the previous prototype, the wire took about 3 seconds to heat up and 25 more to cool down [13]. SMA wire can be used to change wing configurations. For example, it can change the camber of the wing for optimal conditions during take-off, cruising

and landing.

The purpose of this internship research is to find out if SMA wire is a feasible actuator for a morphing wing. This question will be answered by building a prototype and testing it by both table and wind tunnel tests. This report will first discuss the background information about morphing wings and the theory behind SMA in chapter 2. Then a description of the design process will be given. Design considerations and the properties of different concepts will be stated and compared in chapter 3. The chosen concept is then manufactured and tested in chapter 5. The results will be given and discussed in chapter 6. Finally, an answer about the feasibility of SMA wire as an actuator in a morphing wing will be given in chapter 7. After this recommendations will be given. These include lessons learned during this project and how to increase the technology readiness level of the morphing wing.

# Background study

This chapter will review the theory about SMA and morphing wing. The theory behind the theoretical model will also be explained.

## 2.1 Shape Memory Alloy

SMA's are a type of material that have the ability to remember a previous shape. When a SMA is deformed while it is in the martensite state it will only recover the elastic part of the deformation. However, when the material is heated up to the austenite transformation temperature, the material will return to its original shape. This ability is called the Shape Memory Effect (SME) [11]. The most well known alloy to exhibit this behaviour is NiTi [14].

### 2.1.1 SME cycle

The SME cycle goes as follows. Starting from the Austenite parent phase A (see figure 2.1) the SMA is cooled down under zero stress and transforms into Twinned Martensite (phase B). A schematic drawing of a twinned structure can be seen in figure 2.2. When stress is applied to the material, the martensite starts to untwin. At point C, the martensite is fully converted to detwinned martensite. The difference in orientation between the compact twinned martensite and the less compact detwinned martensite is what accounts for the increase in length of the material. When the stress is released from the material, it retains most of its length. At point D in figure 2.1 this is about 4%. When the material is heated again, it changes into austenite and the length increase is lost. The change back to austenite starts at point E and ends at point A, which is where the cycle started.

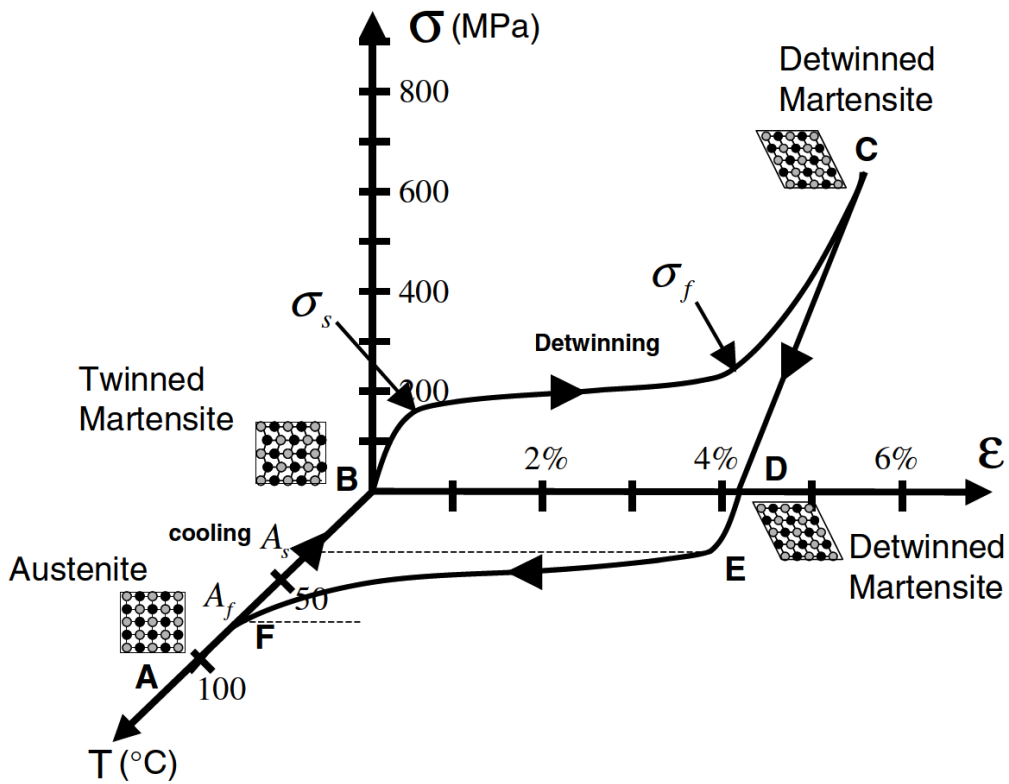


Figure 2.1: Stress-Strain-Temperature Diagram, showing the SME [11].

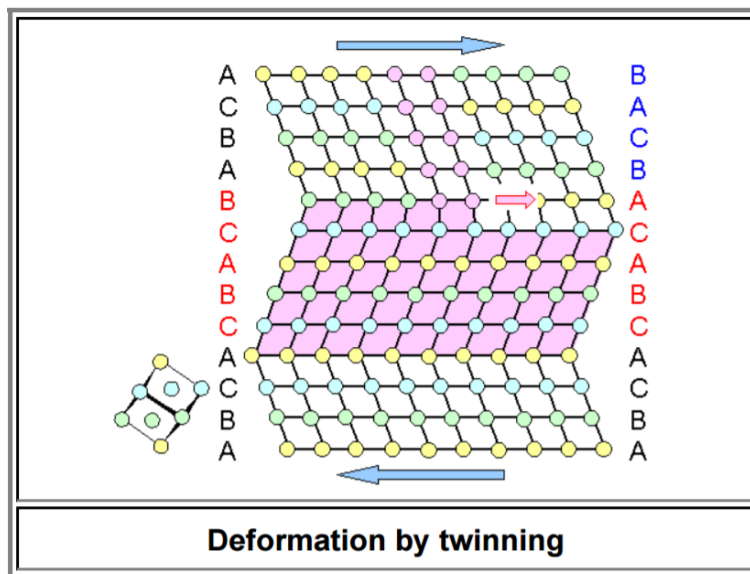


Figure 2.2: A crystal structure in a twinned state [15].

### 2.1.2 SMA training

The first time the NiTi SMA wire transforms from austenitic to the martensitic phase, the orientation of the twinning is random [11]. However, twinning in only the length direction of the wire is preferential. In that case, when the martensite is detwinned, all the increase in length goes to increasing the length of the wire.

The training process is the act of thermomechanically cycling the wire in order to minimize the hysteresis and have a reproducibility of the circles [11]. The Laboratório de Aplicações (LAp) has a set-up to facilitate this process, see figure 2.3. The wires are hung from a beam at the ceiling and a bucket with weights is attached to the lower end of the wires. The wires are then connected to a circuit with an arduino, who controls the passage of the current through the wires. It allows current to pass for 3 seconds. The time and current flowing through the wire need to be exactly enough to heat the wire up to the austenitic phase. When the wire is heated up more, the SME can be lost. The wire transforms to the austenitic phase and shrinks, lifting the weight in the bucket. Then the wires are allowed to cool down for 20 seconds, transforming back to the martensitic phase. Because of the stress that is placed on the wires by the weight in the buckets, the wires will elongate and detwin. By repeating this cycle for two days, the orientation of the twinning will change towards the length of the wire. The cycling also stabilizes the response of the NiTi wire, see figure 2.4.



**Figure 2.3:** Wire training setup in the LAp [16].

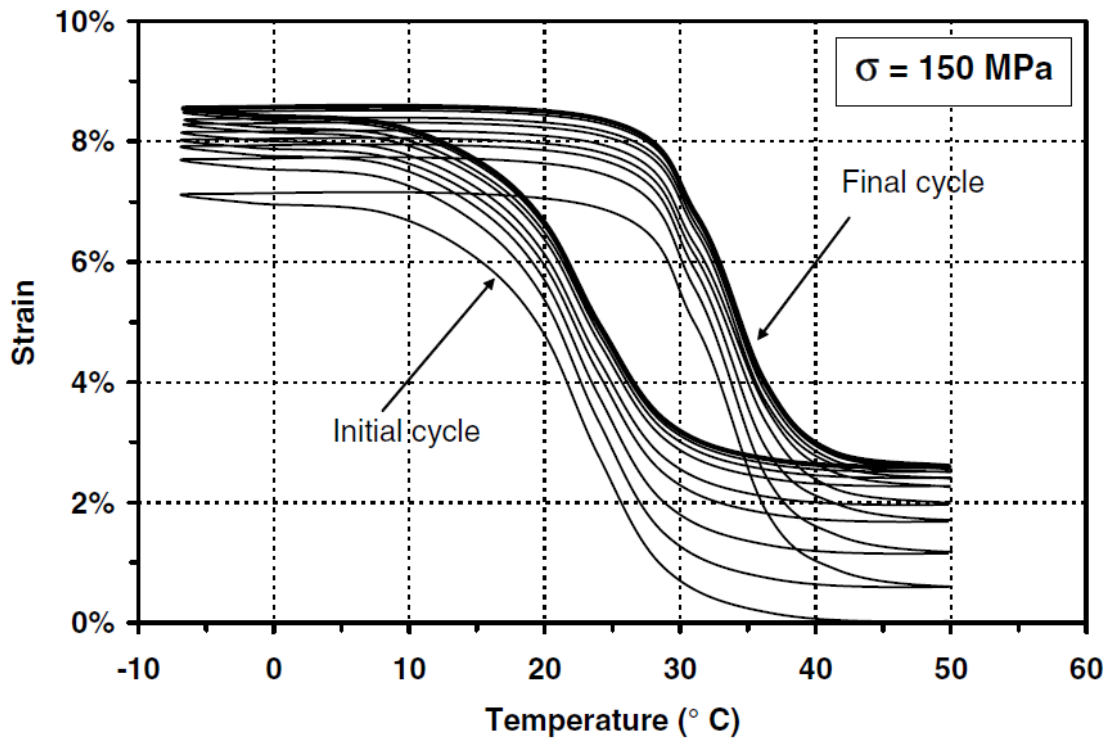


**Figure 2.4:** Stabilizing NiTi wire response by thermal cycling [17].

### 2.1.3 SMA actuator

A wire exhibiting the SME effect can be used as an actuator. There are two different systems for this, see figure 2.5.

The compliant mechanism uses a spring to deform the cold SMA wire back to its detwinned state. When the SMA wire is heated to the austenite phase, it has a higher Young's modulus, allowing it to overcome the force exerted by the spring and shrink.

A second way actuating mechanism uses an antagonistic principle. Two SMA wires are placed opposite to each other. The heated wire is stronger and will pull the cold wire. The antagonistic method has one big advantage over the compliant mechanism. The compliant mechanism needs to continuously heat the wire in order to keep the actuated position. The antagonistic principle does not need this, since one wire will stay in a longer, detwinned phase and the heated wire may cool down to the shorter, twinned phase. However, when the antagonistic mechanism is not heated, it will not be able to resist as much force as the heated variant, because of the lower Young's Modulus.

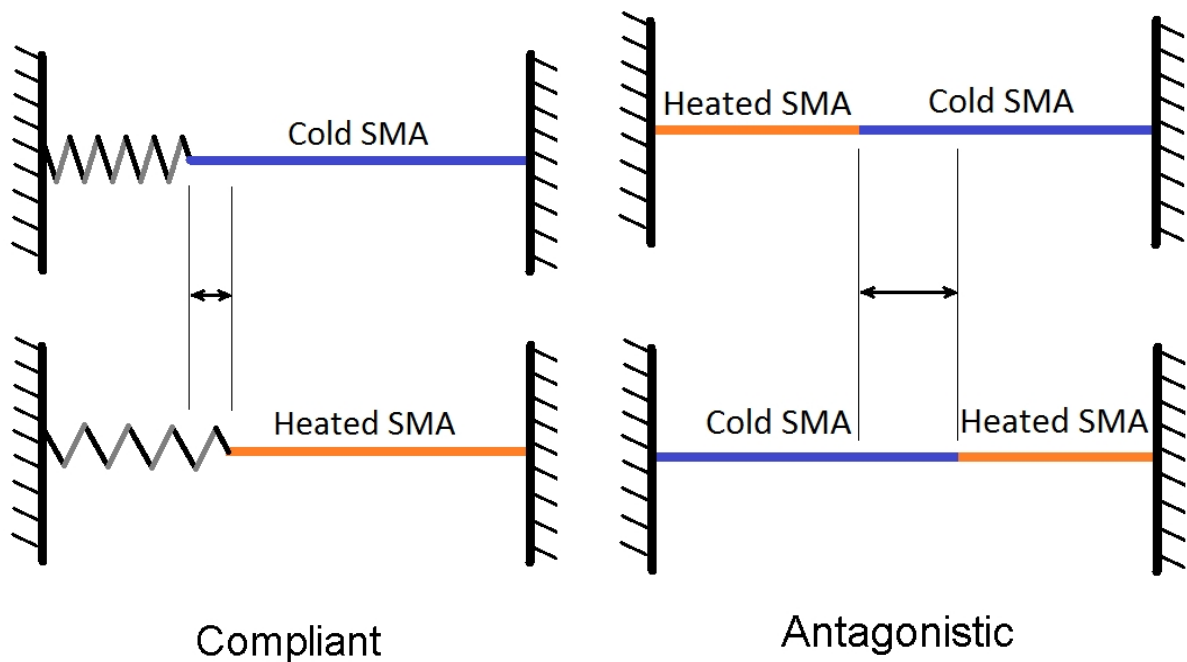


**Figure 2.5:** Two mechanisms for using SMA wire as an actuator [8].

## 2.2 Morphing Wings

Although interest in morphing wings is something that has surged in the past years, morphing wings are not an invention of recent years. For example, the flying machine that the Wright brothers developed had morphing wings. Controlling the aircraft was done by pulling a series of ropes that warped the compliant wing, allowing the aircraft to steer [18]. On later aircrafts this was changed to ailerons, because it was more effective and less complicated than warping wings. Higher flight criteria in modern times have caused morphing to return. The aircraft wing is often designed to function optimal in a specific situation. The delta wing of a fighter jet for example, functions optimally when flying supersonic, but is not efficient at subsonic speeds and does not provide enough lift to fly at low speeds, resulting in difficult landings at high speed. The F-14 fighter jet sought to remedy that, being the first fighter jet with a variable wing. This wing could pivot, making it long and slim for increased lift during take-off from the short airstrip on the aircraft carrier. The wing would then change its angle depending on flight conditions, ultimately resembling a delta wing at super sonic speeds.

More recent examples can be found in the DARPA program. In 2002 DARPA started the Morphing Aircraft System (MAS) Program [18]. Two finalists were selected: The Lockheed Martin Company aircraft design concept, shown in figure 2.7 and the morphing concept of the NextGen Aeronautics Corporation, shown in figure 2.8.

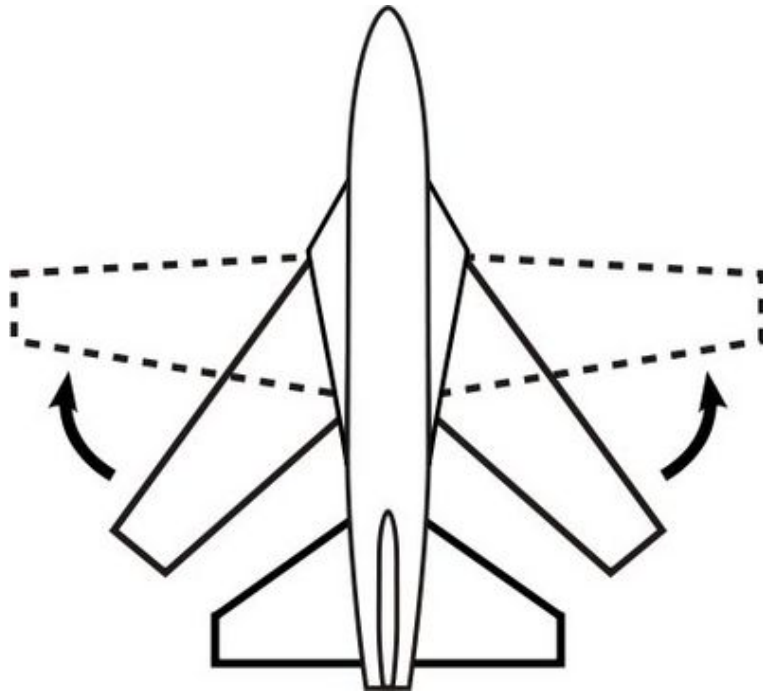


**Figure 2.6:** Schematic illustration of the variable configuration of the F-14 wings.

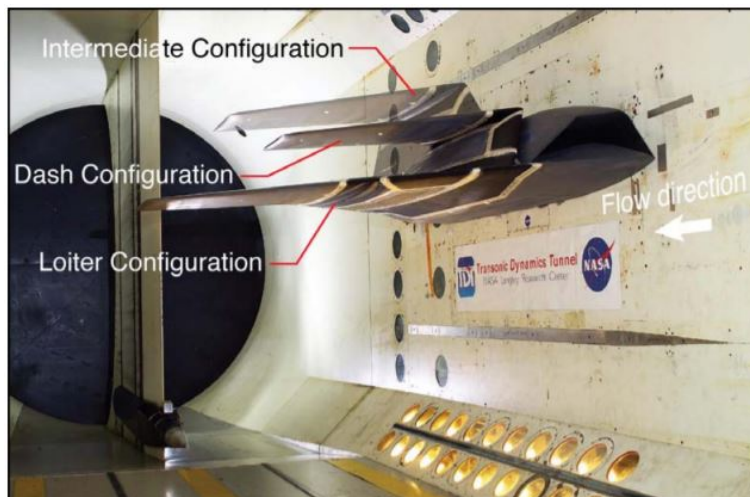


**Figure 2.7:** The different states of the morphing concept of Lockheed Martin [19].

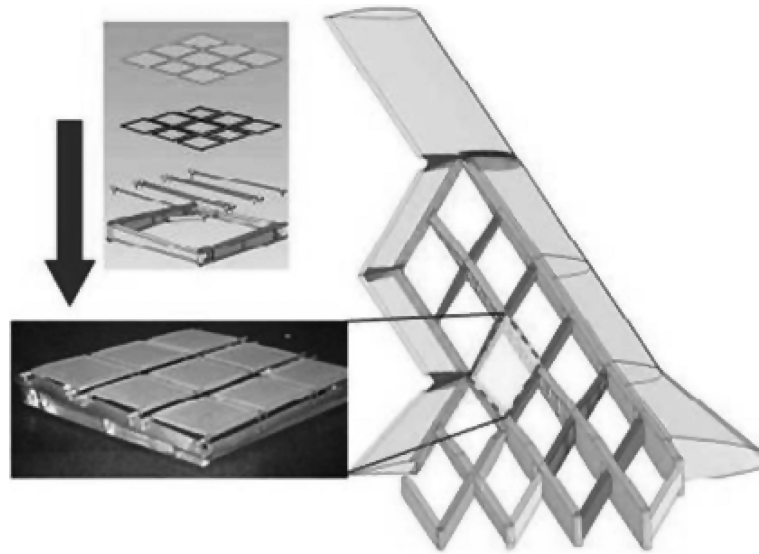


**Figure 2.8:** The morphing wing mechanism of NextGen [18].

The Lockheed Martin MAS featured a wing that could be folded. This way the aircraft had two configurations: A loitering configuration and a dash configuration. The folding was done using electrical actuators. The design had some advanced features such as lightweight thermopolymer actuators that closed the gap between the fuselage and the wing in its folded configuration. It also had an elastomer skin to cover the joints. The skin was prevented from wrinkling by a vacuum pump [9] The NextGen MAS concept revolved around a series of linkages operated by hydraulic actuators and covered by a flexible skin. This allowed the wing to take five different shapes, see figure 2.9.

High Lift	Climb	Cruise	Loiter	Dash/Maneuver (baseline)
 <p><b>Wing design</b> L/D ratio 1.45 b/2 = 8.8 ft. S = 17.0sq. Ft.</p>	 <p><b>Wing design</b> L/D ratio 1.39 b/2 = 9.8 ft. S = 22.8 sq. ft.</p>	 <p><b>Wing design</b> L/D ratio 1.23 b/2=7.2 ft. S = 15.8 sq. ft.</p>	 <p><b>Wing design</b> L/D ratio 1.60 b/2 =9.8 ft. S =17.4 sq.ft.</p>	 <p><b>Wing design</b> L/D ratio 1.00 b<sub>dash</sub>/2 = 7.2 ft. S<sub>dash</sub> = 23.9 sq. ft.</p>
<p><i>b = wing semi-span</i> <i>S = wing semi-span area</i></p>				

**Figure 2.9:** The five different configurations of NextGen [18].

The morphing principles of both wings were tested successfully in the wind tunnel and were allowed to enter the third stage of testing [19] [6]. In this stage the morphing airplanes were tested in flight, to demonstrate the ability of the aircraft to morph in mid flight. The NextGen flight tests were a success [6].

DARPA's MAS project ended in 2007 [18]. Although it used some exotic materials to cover the morphing parts, the actuation was done using traditional mechanical methods. The aforementioned examples show that while morphing wings offer a lot of benefits, they come with a lot of added complexity. These examples should be taken into account during the design phase, to make sure the morphing or the prototype is as beneficial as possible, without adding much extra complexity.

# Design

Designing requires creativity and the process can appear like a black box, where requirements go in and a good idea comes out. However, it is a good idea to use a structured approach to make sure the end product is right. First a clear program of functions and demands is defined. Then possible systems to fulfil these functions and demands are considered. Then at least 3 concepts are proposed, to make sure the designer does not get his mind stuck on one solution only. After this, the concepts are compared and the best one is chosen. Because the prototype is fabricated using a 3d printer and FEM software is not available to optimise the design, creating a good working prototype is an iterative process.

## 3.1 Functions and demands

The prototype should be a proof of concept that SMA wire can be used to actuate a morphing wing. To perform that function, it should fulfill the following demands:

- The wing should be able to deflect at least 30% of its surface in a continuous way (as opposed to the disruptive change in angle of a conventional wing).
- The wing must be able to perform an upwards and a downwards movement.
- These movements must have a significant effect on the airflow (shifting the  $C_L/\alpha$  curve).
- The morphing wing should create less drag than a conventional wing with flap.
- The prototype should be simple and easy to manufacture within the short timespan of the internship.

## 3.2 Concepts

Based on the program of functions and demands in section 3.1 three different concepts have been proposed. One concept is from V. Piccirillo [20]. He used this actuating mechanism in his mathematical model of the aero-elastic effects on a SMA actuated morphing wing. This section will discuss the concepts briefly, explaining the mechanism, material and production methods.

### 3.2.1 Concept Tubo Dobradiça

This concept transfers the linear movement of the wire to a rotation. It can be described as a simple one Degree of Freedom (DOF) system. The airfoil does not morph completely but instead has a flap that is attached to a tube. This tube is connected to (ball) bearings and can rotate, similar to a conventional wing.

- high degree of movement (29 degrees with 80mm wire, 5% shrinkage and 16mm rod)
- does not change angle in a continuous way
- added weight due to rod

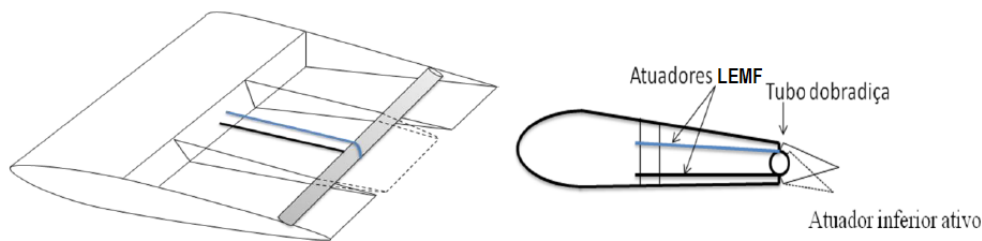


**Figure 3.1:** The SMA wires exert a force upon the tube, causing it to rotate [20]

### 3.2.2 Outwire

The SMA wires are placed outside of the airfoil, giving them a more advantageous position to exert force upon the airfoil, while also getting air-cooled. The airfoil has a wing with a flap, just like conventional airfoils. However, the flap hinge is a cross-flexure to prevent hysteresis.

- acceptable degree of movement (guess: 15 degrees with right dimensions)
- outside wires will be air-cooled faster actuation

- precise control: movement of wire and leaf spring is 100% repeatable (deflection of the flap due to aerodynamical load is not predictable)
- can be light weight
- extensions outwards from the ribs create extra drag.

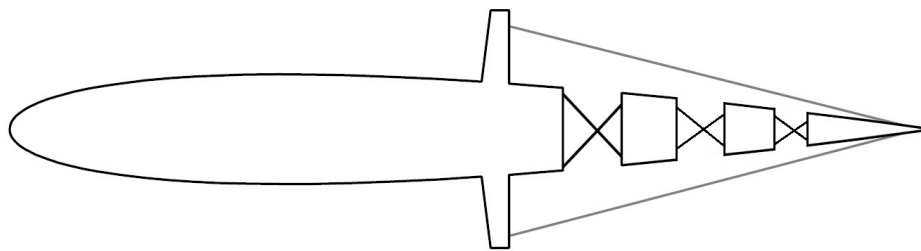


**Figure 3.2:** Concept Outwire

### 3.2.3 Inwire

This concept places the SMA wires inside the airfoil to minimize disturbance to the airflow. The whole airfoil is flexible and able to deform, making for a truly morphing motion. The flexible ribs can be 3d printed.

- morphing wing, best aerodynamic properties
- requires extra actuation force to twist profile
- easy to manufacture with additive manufacturing



**Figure 3.3:** Concept Inwire

**Table 3.1:** Selection criteria

	Inwire	Outwire	Tubo Dobradica
Actuation force needed	-	+	+
Actuation speed	-	+	-
Degree of motion	-	+	++
Ease of manufacturing	++	--	+
Weight	+	-	-
Aerodynamic profile	++	+	--
Total score	2	1	0

### 3.2.4 Selection

To determine the best concept a number of selection criteria have been proposed. These criteria relate back to the functions and demands of section 3.1. The selection criteria, along with the score for each concept can be found in table 3.1.

Importance has been placed on the ease of manufacturing and the aerodynamic profile. Having a functioning prototype with the short timespan of the internship is the most important part. This prototype should prove that SMA wire can be used to morph a wing and that it is more efficient than conventional actuation. The amount of morphing and the actuation force needed can be optimized in later prototypes. Concept Tubo Dobradica is rejected for its lack of morphing capabilities. Concept Inwire is chosen over concept Outwire, because concept Outwire is harder to manufacture because of the leaf springs and the concept creates more drag. This means that concept Inwire will be developed into a working prototype.

## 3.3 Refining ribs

The next step in designing the morphing wing was refining the design of the ribs. A NACA 0012 profile was used, so that the wing was comparable with the wing from Campos de Almeida [13]. If the upper and lower surface of the rib are connected at the trailing edge, the rib does not bend correctly, see figure 3.4. Therefore, the choice was made to separate the upper and lower part of the rib at the trailing edge.

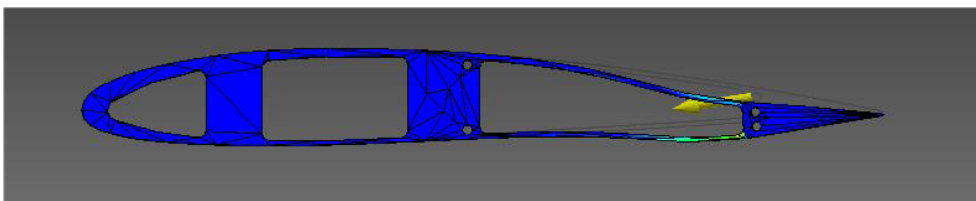


**Figure 3.4:** ANSYS analysis of rib bending [16]

### 3.3.1 Wire placement

The chosen concept, concept Inwire had a couple different possible configurations for the attachment of the wire. The extremes being a 80mm wire attached under an  $45^\circ$  angle and a 150mm wire attached under an  $80^\circ$  angle, see figure 3.6. The  $45^\circ$  angle wire has less length, and therefore will be able to contract less. But the angle under which it contracts is closer to the vertical axis. This should make it more suitable for deflecting the wing vertically and resisting vertical loads. Test were performed to determine the best position to attach the wire. The test set-up can be viewed in figure 3.5.

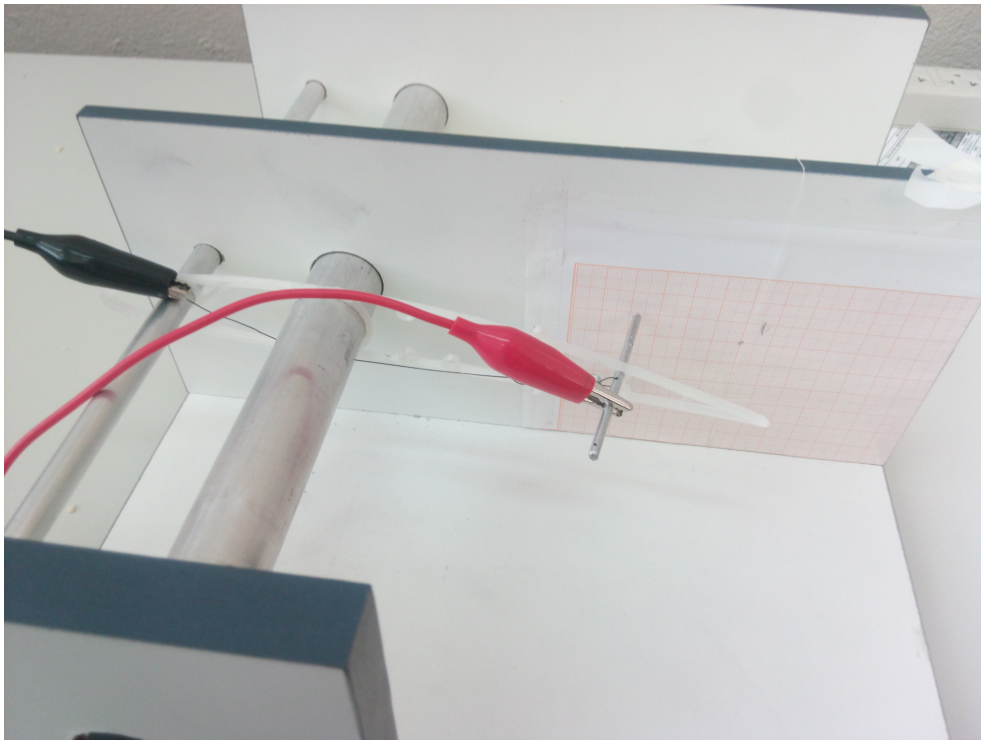


**Figure 3.5:** The test set-up fabricated by [13] used for the measuring of the performance of the morphing wing.

### 3.3.2 Test set-up

The wing cross-section is attached to two tubes, the middle one being  $26\text{mm}\varnothing$  and the left one being  $9.8\varnothing$ . there is also a rod of  $3.5\text{mm}\varnothing$  attached to the right of the wing rib. This rod is inserted into one of the slots of the wing rib. On figure 3.5 the rod is inserted in the last slot and the angle of the wire with the vertical axis is  $80^\circ$ . The SMA wire is attached to the left tube and the right rod using a bolt for the tube and a bolt and a nut for the right rod. The length of the wire can be changed by loosening the nut and clamping it again. The wire is attached to an electric circuit

**Table 3.2:** Results of the wire placement experiment.

	45 (°)	60 (°)	75 (°)	80 (°)
Wire length start (mm)	80	96.5	125	150
Wire length end (mm)	82.5	93.5	121	145
Percentage shrinkage	3.12	3.11	3.20	3.33
Actuation speed (s)	10	6	7	7
Cooling speed (s)	31	28	24	23
Tip deflection (mm)	5	5.5	14	29
Air foil deflection (°)	2.3	2.5	6.4	13.1

by attaching the black clamp to the bolt on the tube and the red clamp to the rod on the right. The other sides of the colored wires are attached to a variable DC power supply. The current is set to 1.4A. This is a current that is save to put on the SMA wire for a long time, without overheating the SMA such that it loses its effect [13].

### 3.3.3 Results

The wires have been attached under different angles from the vertical axis of the 26mm tube. Four configurations have been considered: 45°, 60°, 75° and 80°. These degrees correspond to slots on the profile of the wing, see figure 3.6.

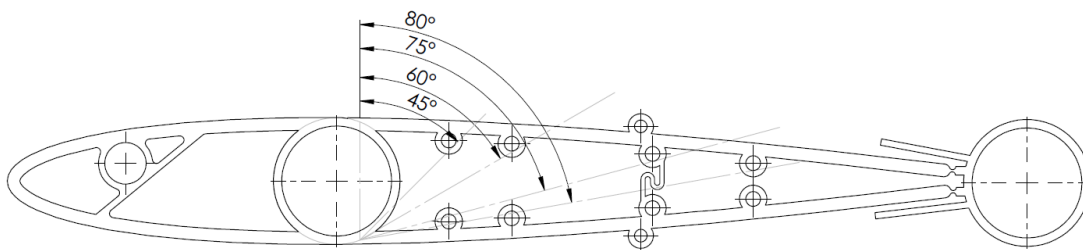


**Figure 3.6:** Drawing of the wing's cross-section, showing the 4 different configurations.

The results of the wire placement tests can be found in table 3.2. Some conclusions can be made. The obvious conclusion is that using the longest wire results into the highest air foil deflection. Therefore the final design will place the attachment points for the wires as far from each other as possible.

The percentage of shrinkage is almost constant. The difference can be explained by the imprecise measurement of the wire length.

## 3.4 Framework

To get the attachment points for wires as far as possible from each other, two attachment points will be placed in the tip of the rib, and two in the 80 ° configuration. At the point where the height of the rib is the largest, the ribs will be connected to a 26mm tube. The ribs will be spaced out evenly along the tube. A 12 mm rod will be connected to the tube, to connect the wing with the wind tunnel. One half of the wires will be connected as demonstrated in figure 3.7.

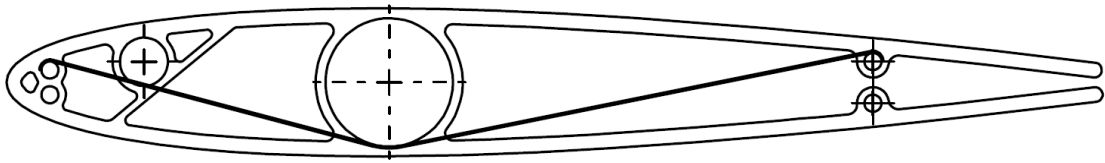


**Figure 3.7:** Picture of the wire clamping mechanism.

The other half of the wires will be mirrored along the length axis of the airfoil. 3.5 mm rods will be placed through the attachment points. These rods are used to attach the wires. The length of each wire will be 170 mm. An extra 50 mm is added to each wire to make it easier to attach the wire to the rods. The total length of SMA wire is 3 m. This allows for 12 wires. The choice is made to attach a pair of SMA wires between two ribs, to create an even force on all the ribs. This results in 7 ribs being needed for the frame. The frame will be 450 mm wide, to be able to fit in the wind tunnel. These decisions result in the frame as can be seen in figure 3.8.

This rendering of the frame shows 3d printed springs that have been added to increase the stiffness against vertical forces. These springs were tested on the test set-up and showed increase in vertical stiffness, while still allowing the rib to morph.

## 3.5 Final Design

The final design is presented here. A technical drawing of the final design of the ribs can be found in figure 3.9. The render of the wing with cover can be seen in figure 3.10.

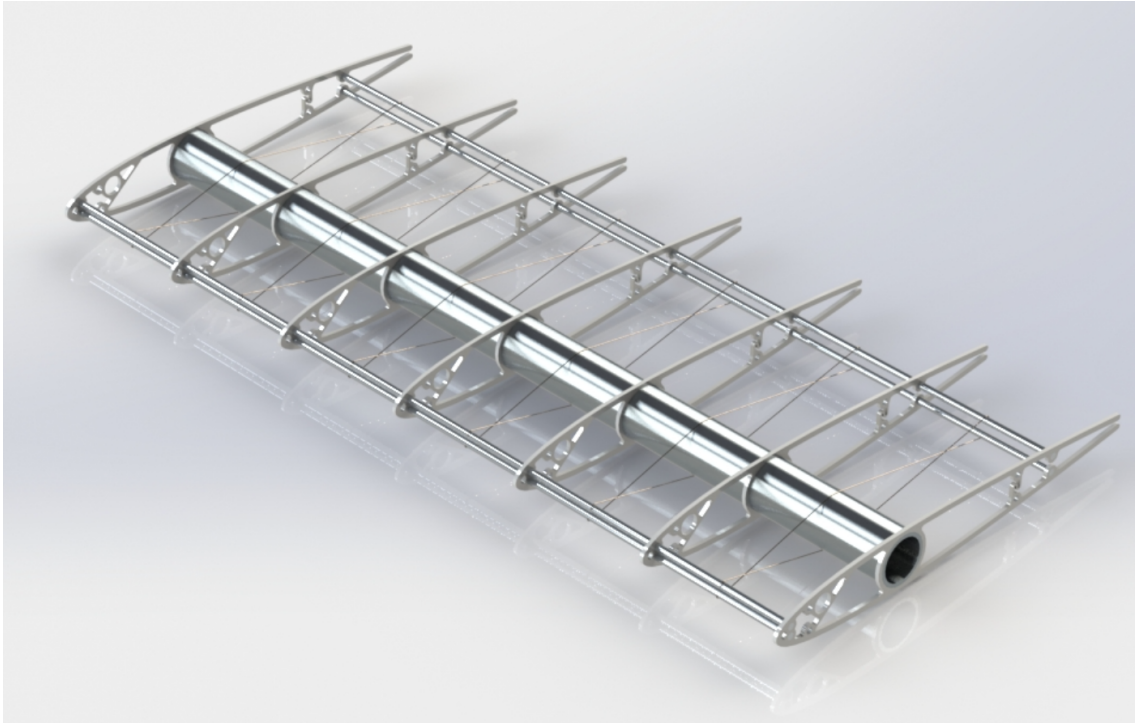


**Figure 3.8:** Render of the wing without cover.

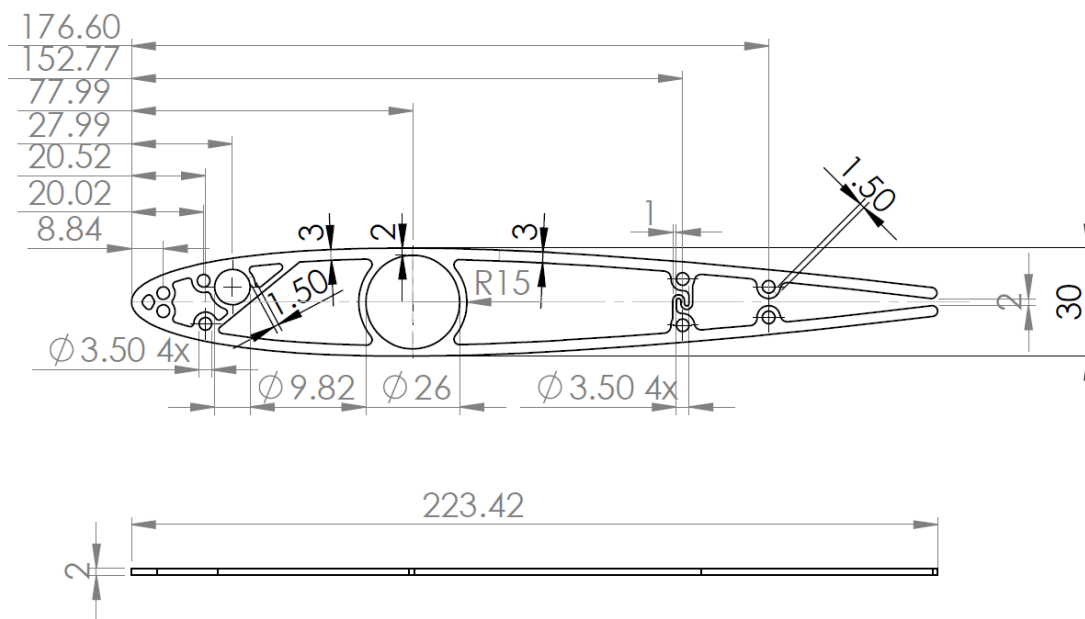


**Figure 3.9:** Picture of the wire clamping mechanism.



**Figure 3.10:** Render of the wing with cover.



# Fabrication

The first part that were manufactured were the 3d printed ribs. They were made by extruding 0.4 mm hot PLA wire. Because this hot wire was used to create a solid object in layers, parts of the object would cool down, while new wire was put on top of there. Because PLA shrinks when it cools down, the whole rib had a tendency to warp upwards, out of plane. To combat this, the bottom of the 3d printed piece had to be glued to the printing bed to secure it while the bed moves. Each new 3d printed layer shrunk a little while cooling, resulting in an out of plane warping of the whole piece. The glue would also let loose at the ends of the 3d printed rib, increasing this effect. This was partially resolved by reducing the thickness of the rib (3mm to 2mm) and designing the rib with extra material at the leading and trailing edges, see figure 4.1. This material was later broken off.

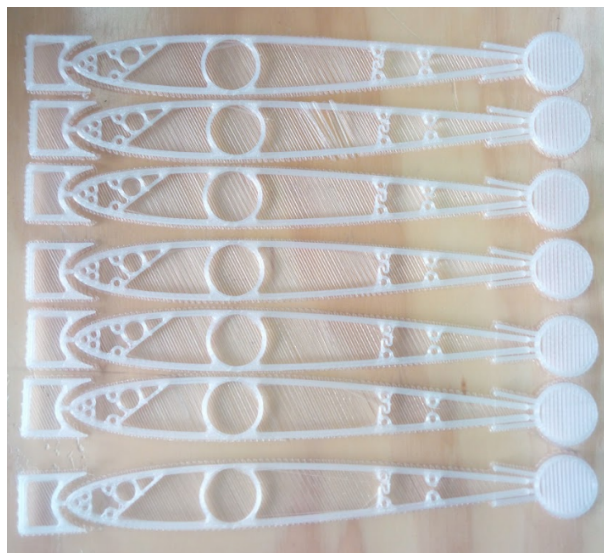


**Figure 4.1:** Picture of ribs as they were 3D printed. The fine structure on the bottom of the pieces was to help create a good foundation for the ribs and was later broken off, together with the front and back piece.

The ribs, tube and rods were assembled without problems. The distance between the rods was determined using the SolidWorks model. The location of the ribs was marked on the 26 mm tube. After the ribs were placed, the location was checked using a 1:1 scale blueprint, see figure 4.2. Afterwards the assembly was secured using solid epoxy glue.

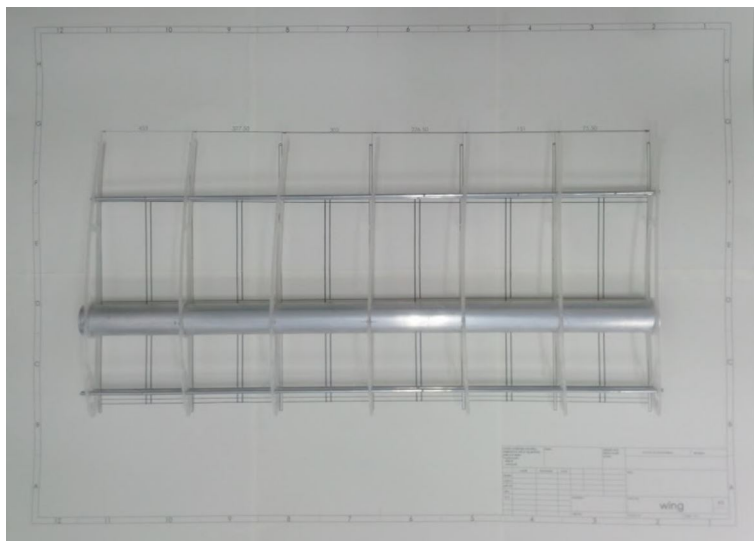


**Figure 4.2:** Checking the rib-tube-rod assembly.

Attaching the wires to the frame proved to be a more tedious task. The choice was made to carve small gutters in the 3.5mm rod and wrap the wire around it and then clamp it with a bolt and washers, see figure 4.3.

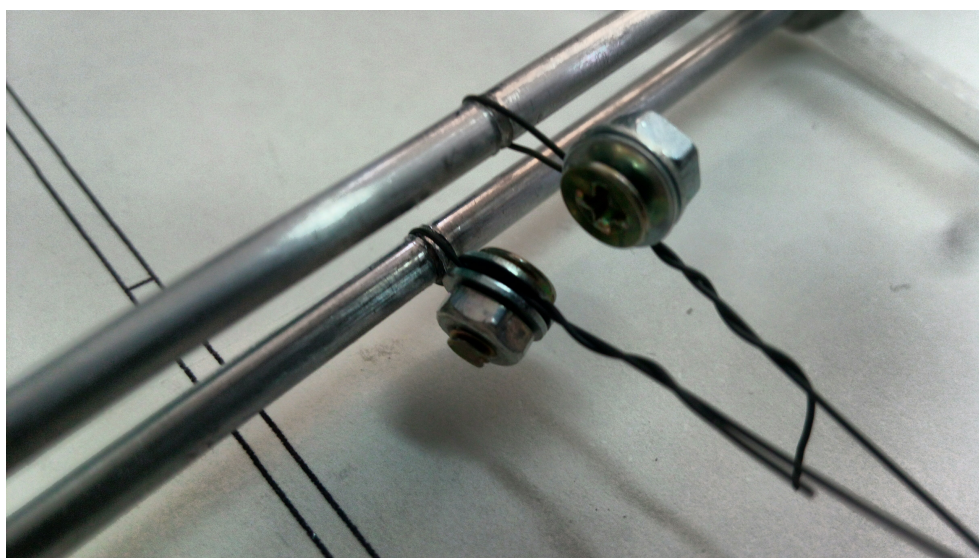


**Figure 4.3:** Picture of the wire clamping mechanism.

Drilling small holes into the rod and pulling the wires through might have been

a better solution. However, this would require a technician, bringing extra cost and delay to the production.

The clamping of the wires required three hands, one to tension the wire, one to hold the nut and one to screw the bolt. This proved to be difficult, since there were only two hands available. In the end, a different approach was found, first tensioning the wire, then wrapping the wire around itself. This way the friction of the wire wrapped around itself would keep the tension on the wire. The way the clamp was placed mattered too. It could be placed either above or below the wire. Depending on how the wire was wrapped and where the clamp was placed, the clamp could twist itself away from the wire. The clamps were first placed in such a way that they would twist to the wire, making the attachment process easier. However, later it was found out that some of the clamps touched each other, see figure 4.4.

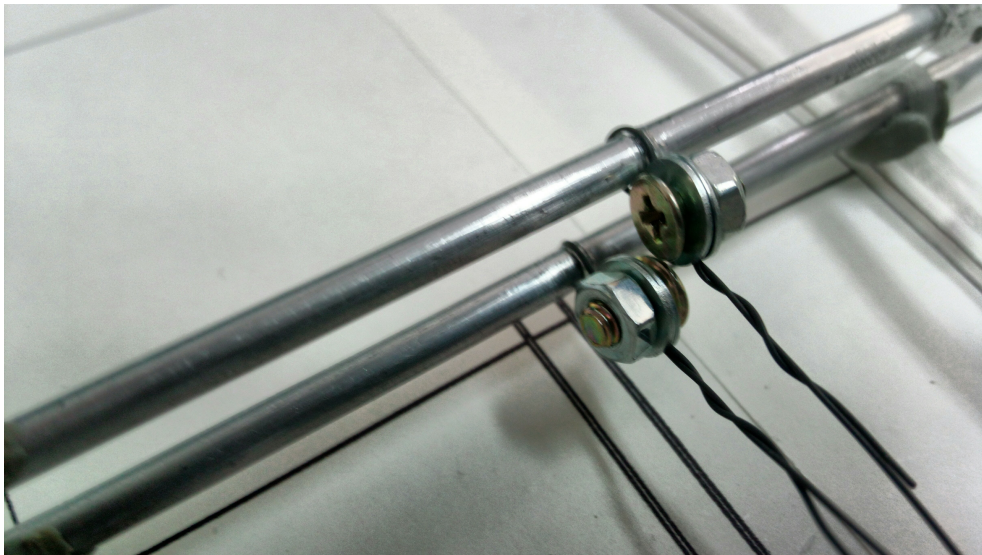


**Figure 4.4:** Picture of the wire clamping mechanism.

This contact could not happen, since two circuits are made, one to actuate the upwards movement of the wing and one to actuate downwards. Therefore the clamps were reattached to make the distance between the clamp of the upper wires and the downward wires maximal. Another point of contact was the contact between the wires and the 26 mm diameter tube. These points were isolated using isolation tape. The contact between the tape and the hot SMA wire was tested using the test set-up of figure 3.5. The isolation tape was able to withstand the wire temperature of 120 °C without problems.

The plan was to use the 3.5 mm rods as conductors, using them to guide the current to the wires. At the first test it became clear that the contact between the SMA wires and the 3.5 mm rods was insufficient and the current was not flowing through. Therefore all the wires were removed. The first 30 mm of the ends of the

wires were twisted with copper wire. This twisted wire was then wrapped around the 3.5 rod and secured with a bolt, just like before.

The contact point with the rod was soldered. After all the wires were secured all the soldered point were soldered to an electric wire. This wire was then used to conduct the electricity from the DC power supply to the SMA wires, see figure 4.5.

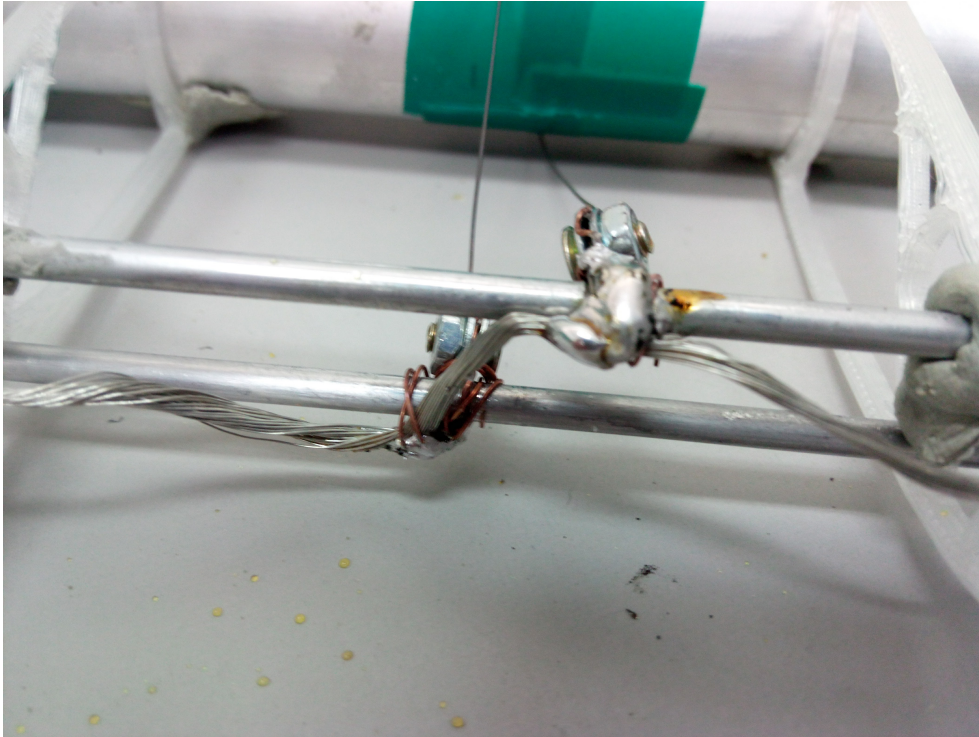


**Figure 4.5:** Soldering at the front end of the wing.

Securing and tightening the SMA/copper wire combo proved to be even more difficult. The result was that some wires were not tensioned enough. The wires were tensioned more by displacing them to the right and then securing them in place with epoxy glue, see figure 4.6.

The grooves in the bottom and the upper 3.5 rods were designed to be 4mm apart of each other in the horizontal plane. This was done to keep the actuation in between the ribs as close as possible to the middle. However, the dimensions of the clamping bolts were not taking into account. The 4mm between the upwards and downwards actuating wires proved to be too little and some of the bolts were touching, even though their were assembled as far apart from each other as possible. This was solved by wrapping the lower bolts in isolation tape, see figure 4.7.

The next time current was passed through the wires, all the wires on one side contracted and the frame was able deform significantly, see figure 4.8. Also visible in the figure are the remains of the cut off vertical springs and an extra line of isolation tape over bottom section of the frame, to make sure there was no contact between

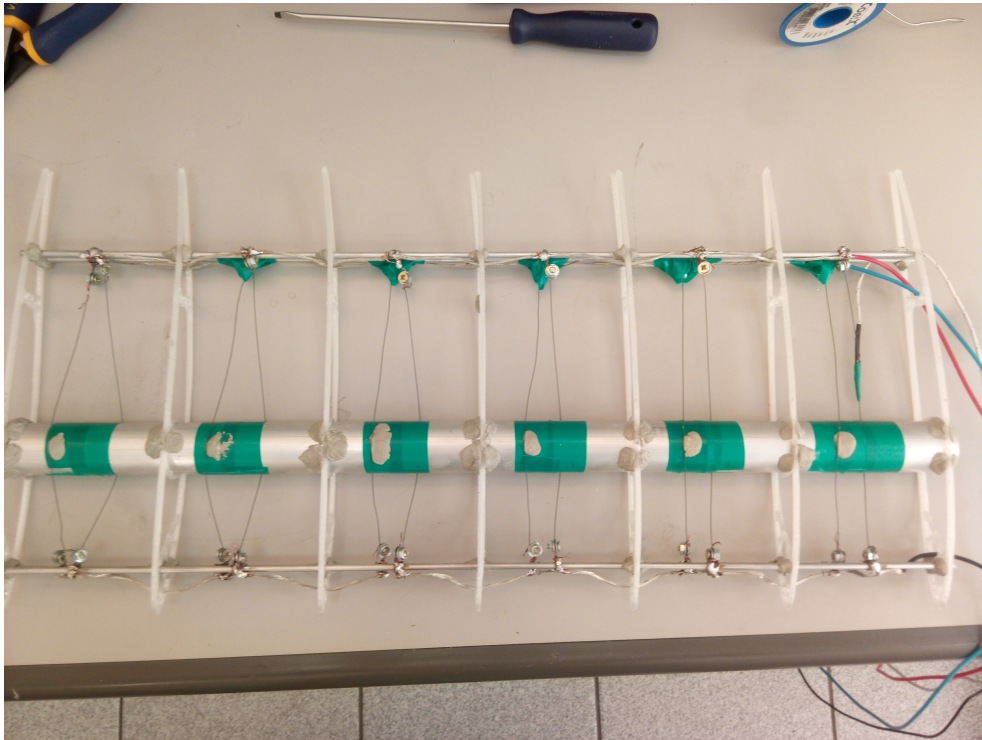


**Figure 4.6:** Topdown view of wingframe. The wires are displaced to the left over the 30mm tube. The insulation tape covering the lower bolts is also visible

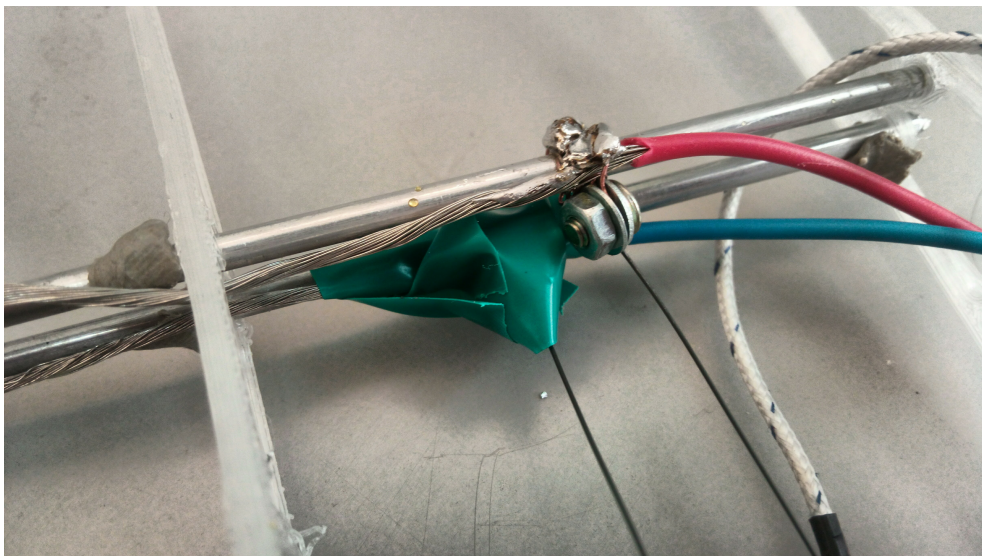


**Figure 4.7:** Picture of one of the bolts covered in isolation tape.

the upper and the lower circuit.

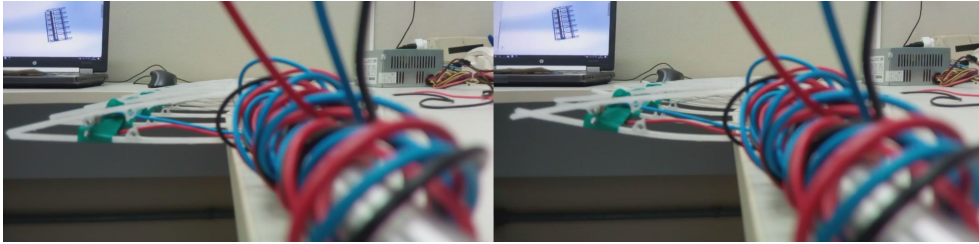


**Figure 4.8:** First successful bending test of the frame.

After the successful bending test, the frame was taken to the wind tunnel to make sure the wing would fit in the wind tunnel. The frame was outfitted with a 12 mm rod that was machined with one end that would fit into the 26 mm tube and another end that would fit into the force moment balance of the wind tunnel. The tube had to be ground down 2 mm lengthwise, to enable the passing of the electrical wires and the frictionless changing of the angle of attack of the wing.

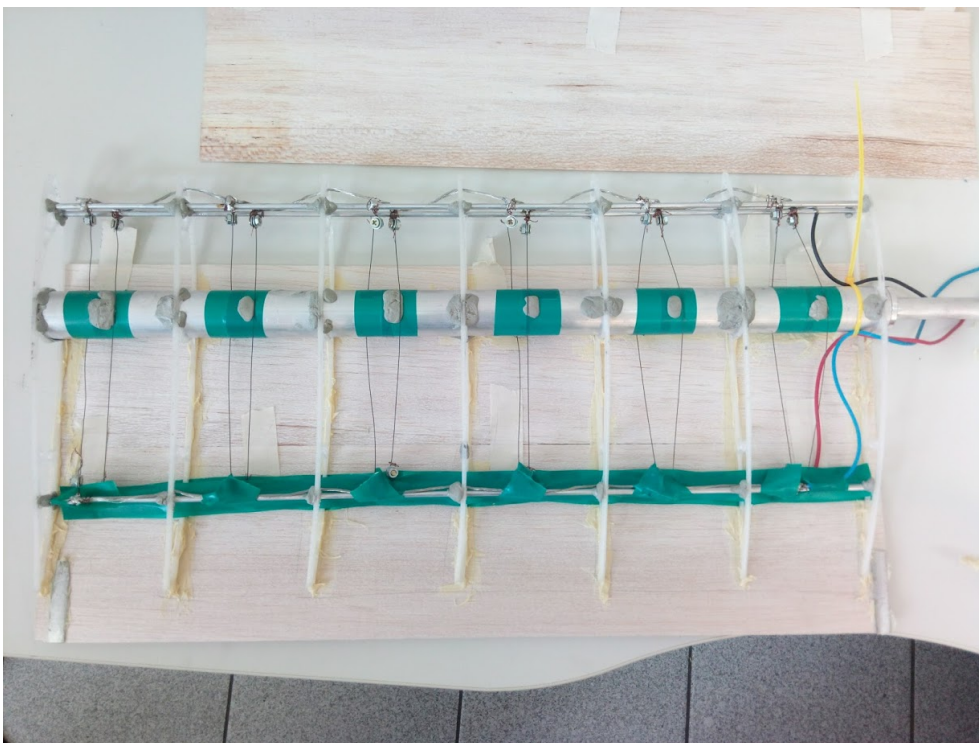


**Figure 4.9:** First panel with protective strips at the trailing edge

The next step was to attach the skin to the frame to finish the wing. The wood was bought as 1000x95x1.5mm and was cut into pieces of 455x95x1.5. 3 panels proved to be enough to cover the whole frame. The panels were aligned and connected with masking tape. The location of the ribs were marked on the wood, since the all purpose glue had to be applied to both the wood and the PLA ribs. Small

aluminium strips were glued at the trailing edge, to protect the thin wood, see figure 4.9. After the first panel was glued down, the second panel was sprayed with water, to make it able to follow the curvature of the leading edge. A small 1mm gap was left between the first and the second panel, to enable expansion of the wood due to morphing. The attachment of the second panel proved to be more difficult because of the curvature and the wetness of the wood. This caused the binding between the glue and the wood panel to worsen. However, the attachment proved to be successful. The third panel glued, with a 2 mm gap between the 2nd and the 3rd panel this time, to align the top and bottom trailing edges. The result can be viewed in figure 4.10.

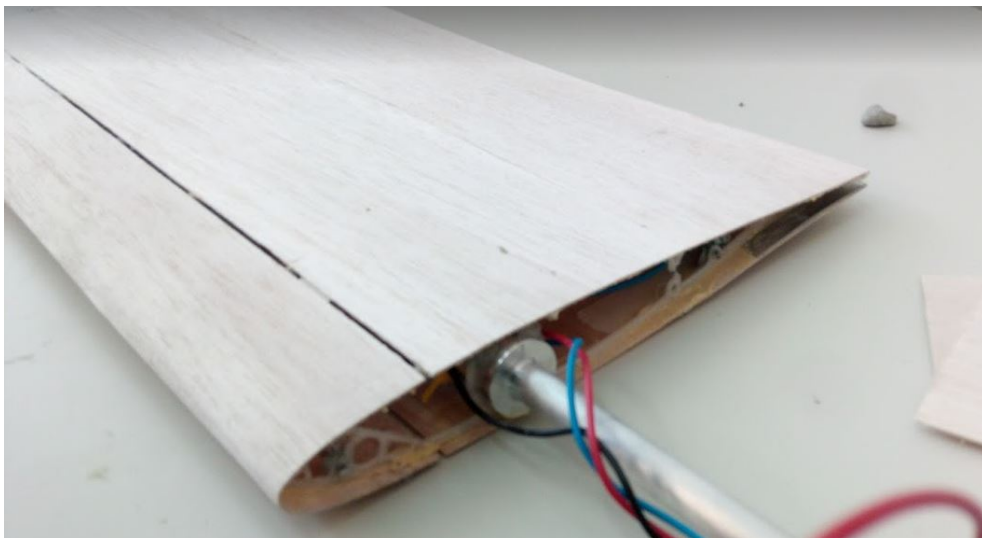


**Figure 4.10:** Wing with wood skin attached

The bending properties of the wing were tested again. Unfortunately, no scale was used, so the result are incomparable with the test results of the completed wing.



**Figure 4.11:** Bending test performed of frame with wood skin.

The wing was sanded down with increasingly higher grit( up to 800) to ensure a smooth surface. The sides of the wing were sanded down to be perfectly perpendicular with the leading edge. The trailing edge was also sanded to remedy a small misalignment between panel 1 and 3. The 1 mm gap was filled with white glue. The

2 mm gap at the top proved to be too big for white glue and was filled with silicon. The sides were outfitted with latex connected by super glue. After this the wing was finished. The result can be viewed in figure 4.12



**Figure 4.12:** Image of the wing in its finished form.

# Testing

This chapter will discuss the testing that has been done to verify the validity of the prototype as an actuating morphing wing. Both the methods used in the table and the wind tunnel experiments will be explained.

## 5.1 Table testing

The wing has two sides covered with latex. One side is where the rod is connected and the other side is free. This side was used to measure the deflection of the wing. The deflection was analysed with the matlab function `imfindcircles`. This function detects circles in an image and returns the radius and location. Therefore, the upper edge of the wing was covered with 13 dots, see figure 5.1. A ruler was fixed next to the wing, in order to provide a scale for the movement. Then the wing was deflected by passing a current through the red and the black electric wires. This current was provided by a 5V 16A DC power source. The current passing through the wires caused them to heat up and shrink, deflecting the wing upwards. The movement of the wing was filmed by a camera in 720p with 29 frames per second. This video was then converted to individual jpg images. The matlab function `imfindcircles` was calibrated to detect the position of the circles in each of the images and a code was written to read the images one by one and store the position of the dots in a matrix. This information was used to plot the movement of the tip of the trailing edge over time and to show the change in position of 13 parts in the wing. This test was repeated for the downwards deflection, by connecting the power source to the blue and black electric wires. The 13 dots were then placed on the underside of the wing, see figure 5.2. The room was a bit darker then, which is visible in the figure. This caused the measurements to be less accurate, as can be seen in chapter 6.



**Figure 5.1:** One of the images used to analyse the upwards movement of the wing.



**Figure 5.2:** This image shows the set-up used to analyse the downwards movement of the wing.

## 5.2 Wind tunnel testing

The wing was tested in the wind tunnel to see if the morphed states of the wing had any effect on the lift and drag coefficient of the wing. The test was done in Professor Feng Laboratory that belongs to Aeronautic Engineering Division from Instituto Tecnológico de Aeronáutica (ITA) in a subsonic blower-type wind tunnel of open loop with internal dimensions of the test section 457 mm x 457 mm x 1200 mm, see figure 5.3. The maximum velocity achieved at wind tunnel is 30.6 m / s. The level of turbulence of the tunnel was 0.5%.

### 5.2.1 Description of equipment

The grey machine on figure 5.3 is used to tune and strengthen the signals from the strain gages, see figure 5.4 and the pressure sensor. It then sends the signals through a converter to the laptop. The grey column, barely visible on the picture is used to see the pressure in the tubes. This pressure is measured with a water column pressure gage. The level of the water column can be read from the grey column.

The wind tunnel was outfitted with a force moment balance, see figure 5.4. This balance had 3 strain gages. Two on the top to measure the lift force and the lift

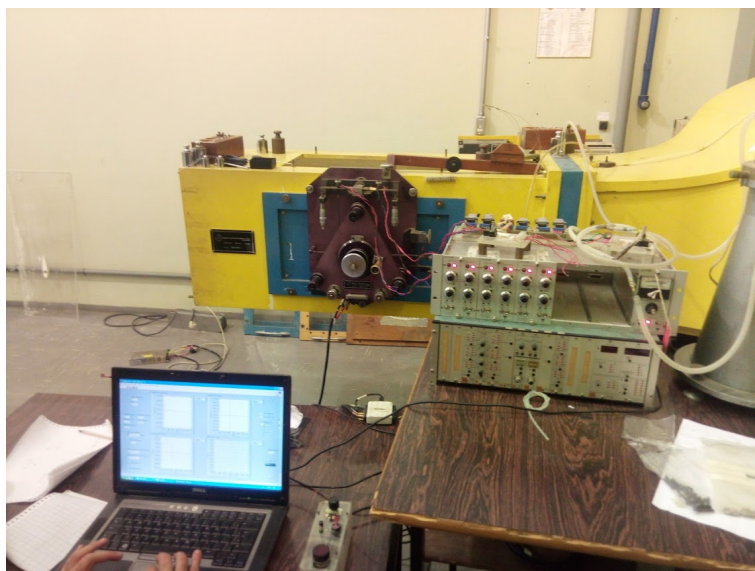


**Figure 5.3:** Equipment at the wind tunnel.

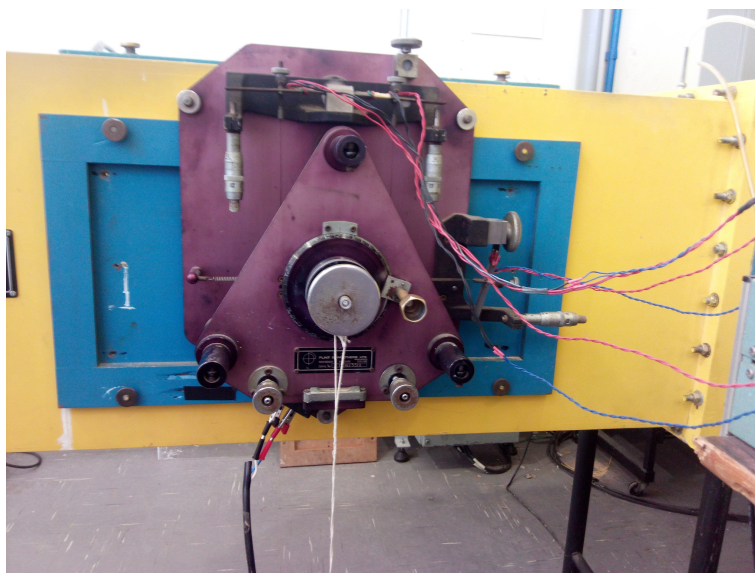


**Figure 5.4:** The force moment balance used to analyse the behaviour of the wing in the wind tunnel.

moment around the 12 mm diameter rod that was used to connect the wing to the force moment balance. The other strain gage was used to measure the drag.

The white rope visible on the image carried a 1 kg weight that was used to compensate the moment generated by the weight of the wing in the wing tunnel. The electric wires rising to the force moment balance from the ground powered the shaker. A device that prevents hysteresis during the calibration with the weights. The rod that held the wing could be rotated using the black disk in the middle of the image. This disk had white marks on it with a resolution of 1 degree. The black disk could be fixed in position with the copper colored clamp next to it.



**Figure 5.5:** One of the scales used to calibrate the lift sensors.

## 5.2.2 Calibration

First a calibration rod was inserted into the force moment balance and clamped. The lift sensors were calibrated from -1.5 kg to 3 kg. The drag sensor from 0 to 650 grams. This was done by connecting scales to the balancing rod and loading them with weights, see figures 5.5 5.6. In order to achieve negative weights, a scale was attached to the outside of the wind tunnel. Load downwards on the rod from the outside of the wind tunnel is the same as load upwards from the inside of the wind tunnel.

First the scale was loaded with 1.5 kg on the scale outside the wind tunnel, then it was loaded with the 3 kg on the scale inside the wind tunnel. The signals were analysed with the 'Sinal Medido #2.vi' software on the computer. The voltage should be around -9 volts for the 3 kg and +3v for the -1.5 kg. This  $12\Delta V$  gives a good accuracy for the measurements. The same process was done for the drag



**Figure 5.6:** The configuration used to calibrate the drag sensor. The pulley converted the vertical load of the weights on the scale to a horizontal load.

sensor, but with either 0 or 650 g on the scale. For the drag sensor, a  $3.5\Delta V$  was needed.

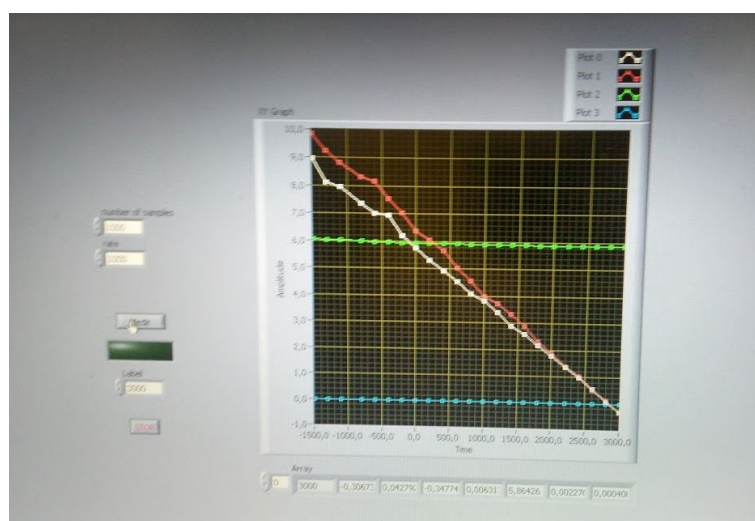


**Figure 5.7:** Calibration of the sensors with linear interpolation between the data points.

After that the real calibration began. The lift sensors were loaded with 200g increments, starting from -1.5 kg. After each load the shaker was activated briefly, to settle the installation. The electric signals were measured using the 'Calibra-Solver.vi' program. After 3 kg was reached, the load on the scale was reduced with 200g increments until -1.5 was reached. This was to check for hysteresis. The same was repeated for the drag sensor, but starting at 0 kg and with increments of 100g.

An example of this calibration can be seen in figure 5.7. Then the pressure sensor was calibrated. The temperature (in Fahrenheit) and atmospheric pressure was read from the sensor in the room. This data was entered into the program. One of the tubes was connected to a hand pump. This pump was used to get the pressure in the tubes to various pressures, specified by the program. The data was entered into the program and a graph was made. The calibration data were combined and loaded into the wind tunnel measuring program 'Aquisição 4 canais\_Red\_v7.vi'

### 5.2.3 Testing

After the wind tunnel sensors were calibrated, the wing was inserted through the force moment balance using the 12 mm rod. The black dial was set to 0 degrees and the wing was levelled horizontally to match the stripe on the inside of the wind tunnel. Then it was clamped tight into the force moment balance. The electrical wires were taped tight to the wall of the wind tunnel, to minimise their influence on the airflow, see figure 5.8.

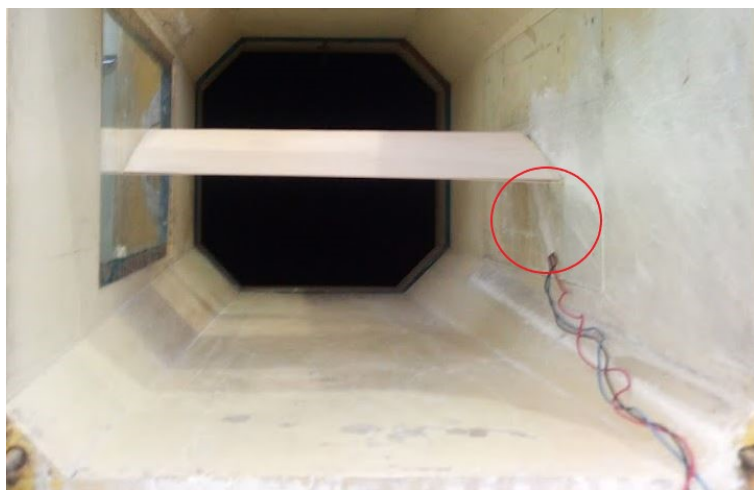


**Figure 5.8:** Morphing wing in wind tunnel. The red circle shows the area where the wires are taped to the wall.

A graph of the shift of center of gravity (cog) was created by measuring the cog of the wing at 0,15,30 and 45 degrees. The shaker was activated at every angle to help combat the hysteresis. The data points were often not close to the plotted line, therefore this process was repeated until a correct graph was generated. After that the test began. The first two measurements gave a negative drag coefficient. Probably caused by the way the wires were taped. The wires were then taped less tight to the wall. Then the cog calibration was done again. After that the first couple drag coefficient values did not go zero. First a test was done with a Reynolds number of about 250,000, but that gave unrealistic results for the lift coefficient, since the

stall point was never reached. The Reynolds number was raised to 450,000. This did provide realistic results. The test started with an angle of attack of -4 degrees. This angle was raised with increments of 2 until after the stall point was reached. After that the test was repeated two more times. The resolution around the stall point was increased by reducing the increments there to 1 degree. Then the blue and black wires were attached to the 5V 16A power source and the same test was repeated 3 times with the same settings, but now on the wing in a morphed state. Subsequently, the blue wires were unplugged and after 30 seconds the red wire was plugged in. This 30 seconds was needed to make sure the actuated SMA wires had returned to the martensite state. After that the test was repeated for the wing in the other morphed state. The laptop started to freeze periodically and therefore the call was made to stop and save the data after only 2 tests of the last morphing state. All of the tests were performed subsequently with the wind tunnel ventilator always on to ensure repeatability and a constant Reynolds number.



# Results and Discussion

The tests presented in the previous chapter had some interesting results. They will be discussed in this chapter. First the results of the table test will be treated. They will be compared to the table test of the rib from section 3.3.2, done in the design phase. The differences will be discussed and explanations of the morphing mechanisms will be given. After that the results of the windtunnel tests will be showed and the consequences of the results will be discussed.

## 6.1 Table test results

When the fabrication of the wings was finished, the first test that was done was a simple actuation test. The results of these tests can be found in figures 6.1 6.2.



**Figure 6.1:** The wing in its downwards actuating position.

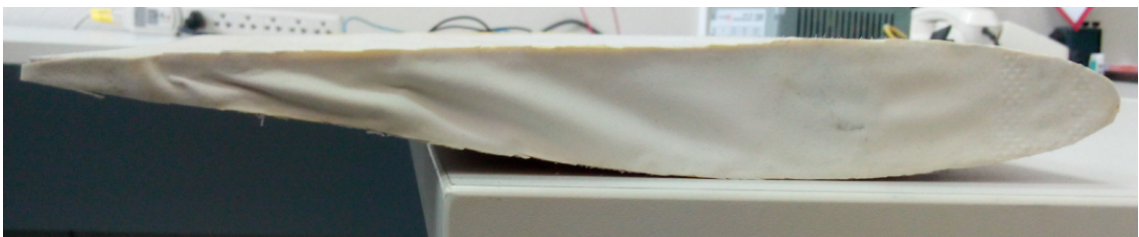


**Figure 6.2:** The wing in its upwards actuated position.

The figures show that the difference between the two actuated shapes is significant. Actuation changes the shape of the airfoil from symmetric to flat on one side and a sharper angle on the other side. When comparing figure 6.2, with figure 4.11 it can be seen that the deflection of the final model is less than that of the wing without latex. This can be explained by the added stiffness caused by the latex and detachment of the rib and wooden skin. This will be discussed in more detail in section 6.1.1.

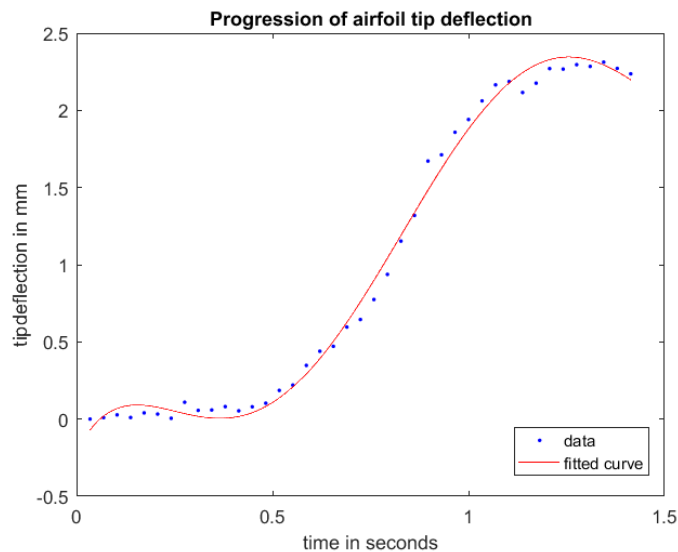


**Figure 6.3:** Graph showing the upwards deflection of the trailing edge over time.

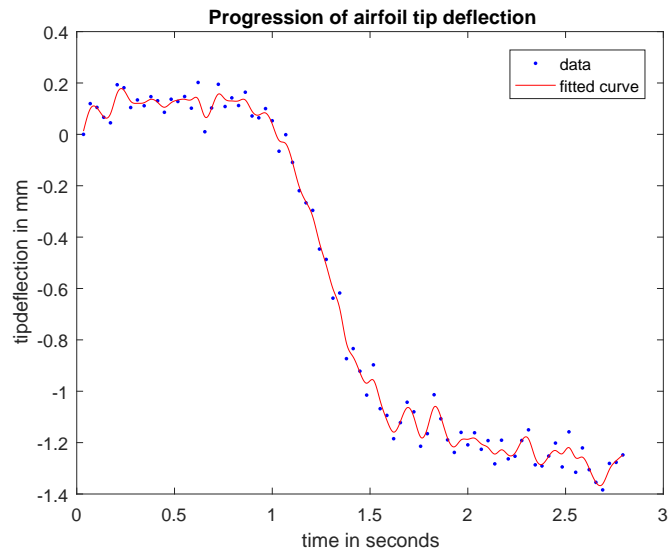
The movement over time of the upwards deflection of the trailing edge tip of the airfoil is shown in figure 6.3. The movement starts at about .5 seconds and ends at about 1.2 seconds. The total deflection of the tip is 2.2 mm.

Figure 6.4 shows the downwards deflection of the trailing edge tip over time. The recording that was used to analyse this movement was made with not enough background lighting. This resulted in a less accurate measurement of the deflection. The downwards movement starts at about 1 second and ends at about 2 seconds. The deflection when averaging the data points is 1.3 mm.

Figures 6.5 and 6.6 show the positions of the 13 points on the edge of the wing during the morphing process. Figure 6.5 is zoomed in so that the reader can see the amount of deflection of each point. In figure 6.6, the ratio is kept original, so that the reader can see the extent of movement compared to the size of the wing. It can be concluded that the movement of the first 6 dots is minimal. This means that only the last 115 mm of the 250 mm wing is really morphing.

Another interesting thing is that the deflection of the end tip is less than the deflection of the dots before.

The deflection of the wing surface is with 2mm not nearly as much as the 29mm



**Figure 6.4:** Graph showing the downwards deflection of the trailing edge over time.

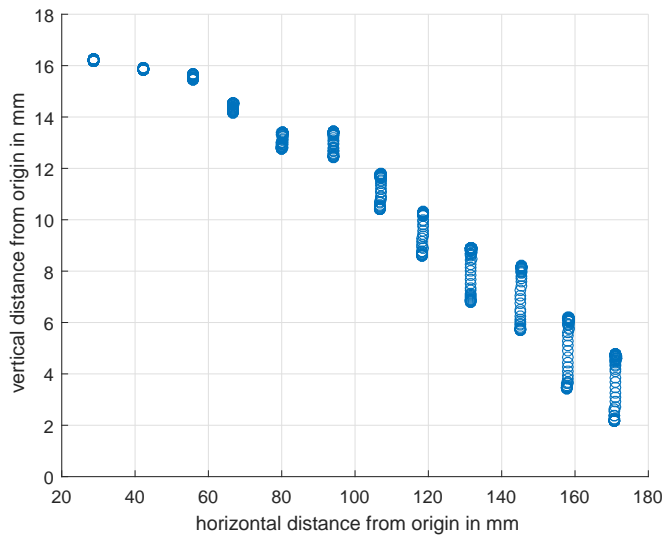


**Figure 6.5:** Graph showing the upwards deflection of the 13 points on the trailing edge.

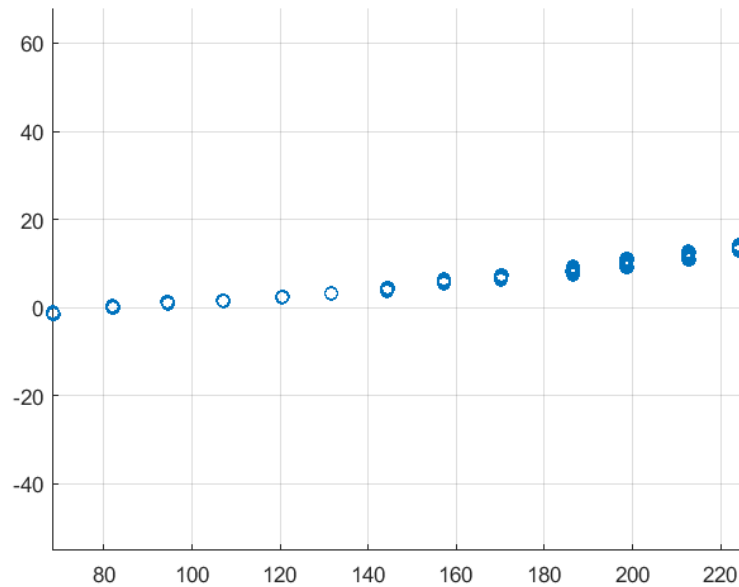


**Figure 6.6:** Graph showing the downwards deflection of the 13 points on trailing edge.

that the rib was able to deflect. There are multiple reasons for this. First the deflection mechanism of the rib will be discussed, then the deflection mechanism in the assembled wing.

### 6.1.1 Rib deflection mechanism

The rib deflection test was conducted with a single SMA wire. It was measured that this wire deflected about 3%. In the 80° configuration this amounts to about 5 mm change in wire length, see table 3.2. The deflection of the tip of the rib however was 29 mm, much more than the 5 mm that the wire changed. On top of this, the best results were with the wire in the 80° configuration. This is almost horizontal. How is this possible? The way that the rib is actuated is as follows: The wire pulls with an 80° angle on the top part of the rib, pulling it towards it. The top part of the rib has to maintain its original length in a shorter space. This causes it to deform like a clamped beam, deflecting upwards, see figure 6.7. The upper part and the lower part will be referred to as beams from now on.

Figure 6.7 is made using SolidWorks drawing. It is tried to make it an accurate representative of the actual situation. The length of the underside of the upper beam until the part where the 3.5 mm rod is connected is 85.89 mm. The length of the beam after the rod is 39.99 mm, not counting the rounded end. In the sketch, the rod is drawn where it would be when the wire retracts 5 mm. This amounts to 2.5%

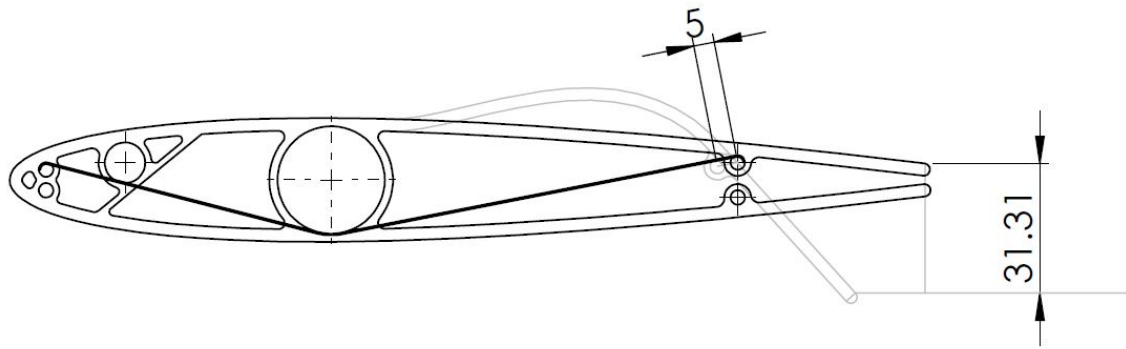


**Figure 6.7:** Vertical deflection of rib in mm when SMA wire shrinks 5 mm (2.5%). The deflection is to scale and is not exaggerated.

shrinkage. This is the maximum achievable shrinkage with the antagonistic wire system, see section 6.2. The beam has to bend to maintain its 85.89 mm in this new state. A spline is drawn to the new position of the rod with a length . The vector of the left side of the spline is set horizontal, to simulate a clamped beam. The size and direction of the vector at the right end is made so that the total length of the spline is as close as possible to 85.89 mm (85.62 mm). After that a 39.99 mm line is drawn with the same angle as the right end vector. When comparing the original vertical position of the upper tip of the trailing edge to the new position, it is found that the difference is 31.31 mm. This value is close to the 29 mm measured in table 3.2. In that test the wire also shrunk 5 mm. Therefore the results are comparable. The difference in length can be explained by the fact that the end part of the rib did not behave like a straight line in the test from section 3.3.3. Instead, the stiffness of the lower beam prevented the upper beam to deflect freely.

This is the bending mechanism for the ribs. In the next section it is discussed what happens with the actuation of the ribs when they are in the wing.

## 6.2 Surface deflection

The surface is glued to the ribs. To protect the trailing edge, metal plates have been placed at the first and last rib. Figure 6.8 shows what happens to the wing when the wire is actuated. The numbers on the figure correspond with the numbers in the enumeration below.

1. The wire retracts, pulling on the rib.
2. The upper beam starts to deflect downwards.
3. Because the wooden surface is glued to the ribs, the glue pulls the surface downwards.

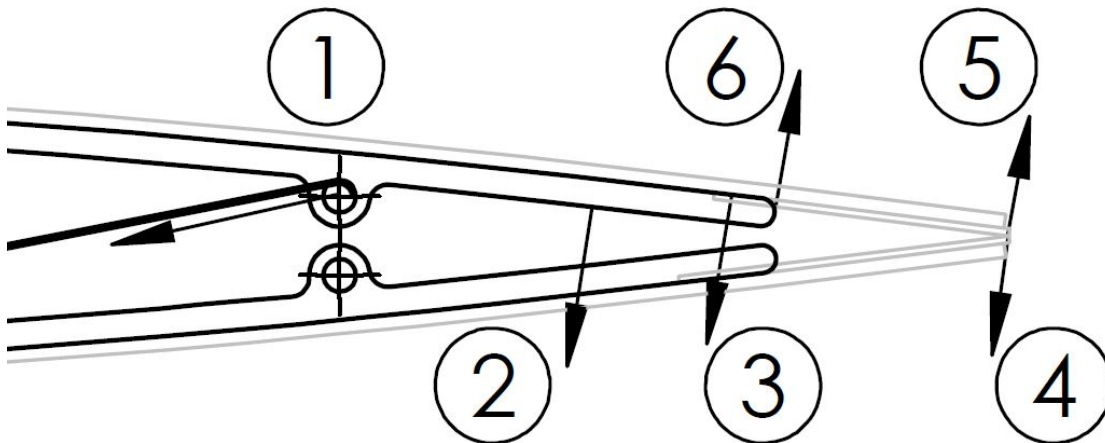


**Figure 6.8:** Explanation of the reduced deflection of the surface.

4. The metal plate of the upper part touches the metal part of the lower part, pushing it downwards.
5. Because the lower part has a certain stiffness, it exerts a force on the upper part, resisting its movement.
6. This force is extended through the stiff metal plate. Because the metal part extends further than the end of the rib, a moment is created. This moment peels of the glue between the rib and the wood surface.

This causes part of the rib to lose connection to the wood surface. Therefore not all of the movement of the rib is transmitted to the surface. This explains why it was observed that the middle of the wing deflects about 4 mm, and the edge of the wing only deflects 2 mm.

This accounts for some of the decrease in deflection, but not for all. A major component of the decrease in deflection has to be caused by the lack of tension in the wires. As discussed in chapter 4, tensioning of the wires proved to be very difficult. The wires were elongated about 8% after the training process, and it was expected that this would help tension the wires. As the wires would shrink that 8%, and then only be elongated around 4%. This process would leave the wires 4% shorter than they were when attached to the frame. However, the first test of the frame showed that the connection between the SMA wire and the rod was not conductive enough. The test caused the wires to be partly heated, losing their 8% elongation. The wires had to be removed and intertwined with copper at the end, and tensioned again. The tensioning of the wires with copper proved to be more

difficult and the wires were tensioned properly. There was a gap varying between 0-3mm between the wires and the 26 mm tube. When the wires shrink, they first have to bridge this gap before they bend the rib. It is believed that this causes most of the loss of the tip deflection.

Another explanation is that the combined stiffness of the wood surface, ribs, antagonistic SMA wires and metal plates is too much for just 6 0.4 mm wires to actuate. In the test from section 3.3.3, there was one SMA wire and one rib. The wire did not have to bend the wood surface and the antagonistic SMA wire as well.

### 6.3 Wind tunnel test results

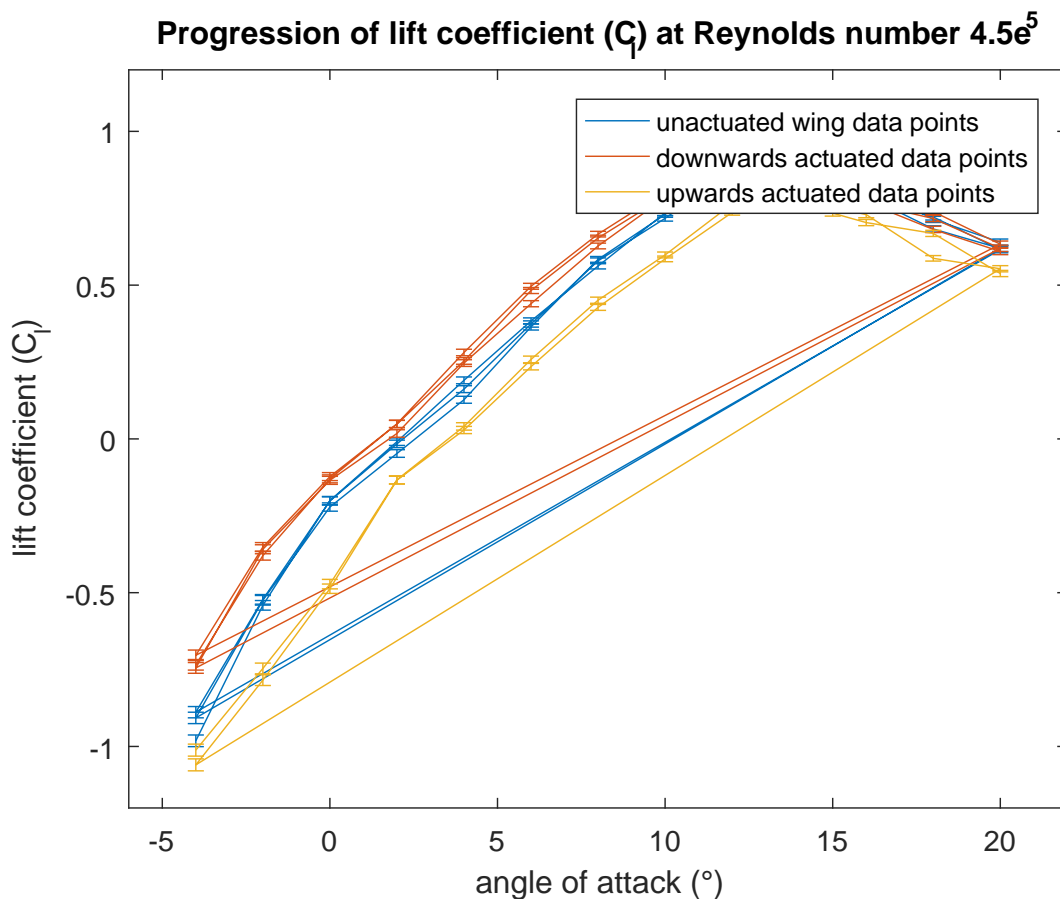


**Figure 6.9:** Lift coefficient plotted for different angles of attack.

The lift coefficient test results are plotted in graph 6.9. As was mentioned in section 5.2.3, there are three test results for the first two configurations and only two for the last one.

The lift coefficient data from the wind tunnel test was plotted using the errorbar function of matlab. For each run, it plots the data point and the error associated with

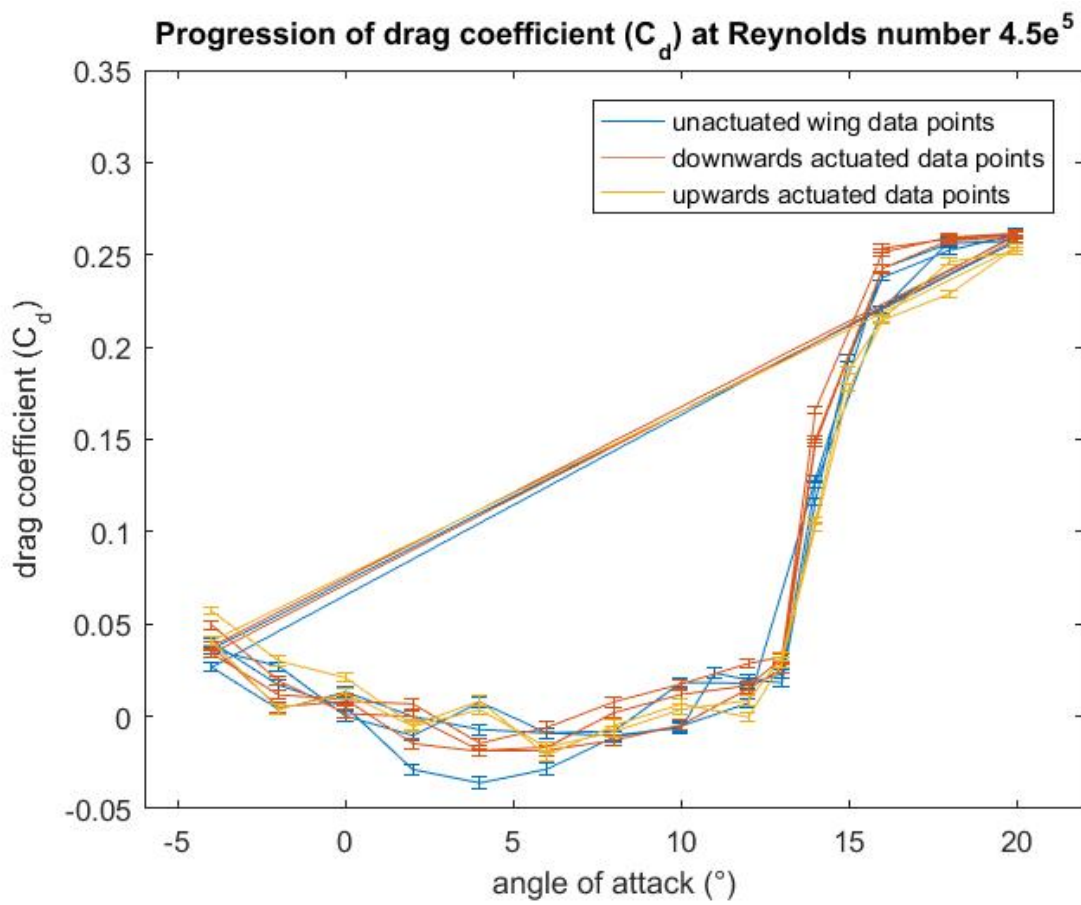


**Figure 6.10:** Drag coefficient plotted for different angles of attack.

the measurement. This error is due to the noise of the electronic signal, caused by the amplification of the strain gage signal.

The graph shows the repeatability in the tests done per configuration. It also shows that there is a clear difference between the morphed states of the wing. This proves that SMA wire can be used as an actuator in a morphing wing.

The drag coefficient data has also been plotted, but the measurements were not very accurate. The drag coefficient even goes below zero. The drag sensor was more sensitive, with a range of 0-600g. This is a factor 7.5 more sensitive than the lift sensor, which was calibrated from -1.5kg to 3.0kg. Several attempts were made to improve the drag sensor before the final test was done, but to no avail. What can be seen in the graph is that the drag increase significantly around  $13^\circ$ , which is the stall point of the plane.

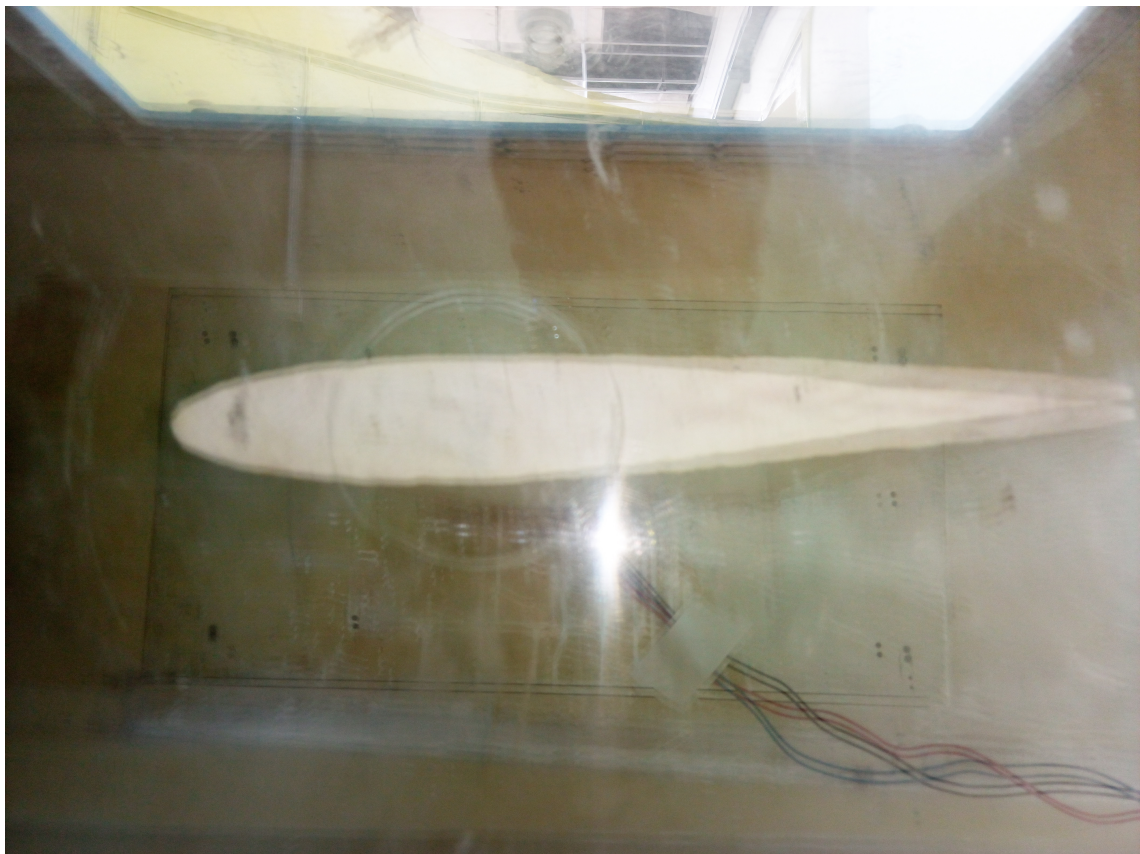


**Figure 6.11:** Overlay of two pictures, comparing the two extreme positions of the morphing wing.

Figure 6.11 shows the difference between the two extreme forms the morphing wing can make. The position where the two photos were taken was not totally equal, as can be seen by the failure of the wires to overlap. The photo therefore shows a slightly exaggerated actuation.



# Conclusions and Recommendations

## 7.1 Conclusions

This research set out to prove that SMA wire can be used as an actuator and in that it succeeded. The tests in the wind tunnel show that even with the 2 mm deflection caused by the SMA wire, the characteristics of the wing change considerably. This proves that SMA is a feasible actuator in a morphing wing. This opens the way for new research into extending the range of motion of the wing and optimizing the morphed airfoil shape. Other forms of morphing, like twisting and sweeping can be implemented too. When a control system is made for the actuation of the wires, a prototype wing could be fabricated and tested on a RC plane.

## 7.2 Recommendations

This project was very interesting and the results show that SMA wire can be used as an antagonistic actuator. However, the wing can be improved a lot to increase its performance. Below a couple changes to the will be discussed that will help get the most out of the SMA actuating principle. Most of these things came to light when fabricating the wing.

In the future a lot more focus needs to be place on building the frame. The ribs have to be extended all the way to the end of the trailing edge, to prevent any unwanted forces that will peel of the glue between the ribs and the surface. The trailing edge tips of the ribs should also have a larger contact surface. This will enable more contact area between the ribs and the surface, giving a stronger connection. On top of that, the upper and lower beam of the rib will be prevented from moving sideways and losing contact. The design of the ribs should be optimized iteratively until a rib is produced that fulfils all these requirements, and does not warp out of plane.

Spacers should be used to guarantee even spacing between the ribs at the lead-

ing edge, middle and trailing edge. This will also prevent the wires from bending the frame sideways.

The connection between the ribs can still be rods and a tube, but the rods should be perfectly straight. The rings that were carved in the rods to attach the SMA wires caused the rod to be less stiff and these points. Therefore the rod bent easily and was not straight. This can be avoided by drilling small holes through the rods that allow the wires to pass through and be connected. The connection of the wires should have a mechanism to tension the wires individually. This could be a spool that rolls up the wire when twisted. This mechanism is similar to that used to tension guitar strings.

More SMA wires should be used. This will help guarantee the maximum possible deflection of the wing. It will also help the morphing wing keep its form when subjected to drag and lift forces.

The wood panels should be tensioned while glued to the wing, preventing hills and valleys in the surface. This appearance of irregularities is also caused by the wood getting wet because of the glue. To prevent this, a different material could be used as the surface cover. For example a thin (1-3mm) sheet of plastic. This will be less prone to forming hills and valleys and does not wet because of the glue. This sheet of plastic can be transparent too. This will make for a good demonstration model and can help people new to the principle understand what is happening. It also helps with studying the mechanism.

The morphing capabilities of the wing can also be expanded. To make the wing a better elevator, the front end of the ribs can be made less stiff. This will allow the leading edge of the wing to bend downwards while the trailing edge bends downwards too. Which will improve the lift coefficient of the wing.

Another extension would be to actuated the wires individually and have them monitored by either a temperature sensor or strain gage. This will help create a feedback loop that allows the wires to be precisely actuated. Because the wires are individually actuated, some can be heated more than others, twisting the wing. The wing twisting can function as an aileron. Because the wires are slow to cool down and return to their original position, this will either cause the manoeuvre to be very slow, or be very large. For surveillance drones, needing to stay in the air a long time, the manoeuvrability matters less than the efficiency.

But to be able to say that the morphing wing is more efficient than a normal flap or aileron, a trade-off study needs to be done. This study will need to compare the energy needed to heat the SMA wires for the manoeuvre to the energy saved by the reduced drag.

# Bibliography

- [1] C. Breitsamter, "AERODYNAMIC EFFICIENCY OF HIGH MANEUVERABLE AIRCRAFT APPLYING ADAPTIVE WING TRAILING EDGE SECTION," 2004.
- [2] S. I. B. Arbarino, O. N. U. R. B. Ilgen, R. A. M. A. Jaj, M. I. I. F. Riswell, and D. A. J. I. Nman, "A Review of Morphing Aircraft," vol. 22, no. June, 2011.
- [3] N. Aeronautics, "Design of a Flexible Skin for a Shear Morphing Wing," vol. 21, no. November, 2010.
- [4] D. Coutu, V. Brailovski, and P. Terriault, "Optimized design of an active extradors structure for an experimental morphing laminar wing," *Aerospace Science and Technology*, vol. 14, no. 7, pp. 451–458, 2010. [Online]. Available: <http://dx.doi.org/10.1016/j.ast.2010.01.009>
- [5] Y. Dong, Z. Boming, and L. Jun, "A changeable aerofoil actuated by shape memory alloy springs," vol. 485, no. 3010, pp. 243–250, 2008.
- [6] J. S. Flanagan, R. C. Strutzenberg, R. B. Myers, and J. E. Rodrian, "Development and Flight Testing of a Morphing Aircraft , the NextGen MFX-1," no. April, pp. 1–3, 2007.
- [7] U. Icardi and L. Ferrero, "Preliminary study of an adaptive wing with shape memory alloy torsion actuators," *Materials and Design*, vol. 30, no. 10, pp. 4200–4210, 2009. [Online]. Available: <http://dx.doi.org/10.1016/j.matdes.2009.04.045>
- [8] V. P. Galantai and V. P. Galantai, "Design and Analysis of Morphing Wing for Unmanned Aerial Vehicles by Design and Analysis of Morphing Wing for Unmanned Aerial Vehicles," 2010.
- [9] D. A. N. Iii, D. J. Inman, and C. Woolsey, "Design , Development , and Analysis of a Morphing Aircraft Model for Wind Tunnel Experimentation by Design , Development , and Analysis of a Morphing Aircraft Model for Wind Tunnel Experimentation," 2006.

- [10] A. Y. N. Sofla, S. A. Meguid, K. T. Tan, and W. K. Yeo, "Shape morphing of aircraft wing : Status and challenges," *Materials and Design*, vol. 31, no. 3, pp. 1284–1292, 2010. [Online]. Available: <http://dx.doi.org/10.1016/j.matdes.2009.09.011>
- [11] D. C. Lagoudas, *Shape Memory Alloys Modeling and Engineering Applications*. New York: Springer, 2008.
- [12] D. M. Elzey, A. Y. N. Sofla, and H. N. G. Wadley, "A bio-inspired , high-authority actuator for shape morphing structures," vol. 5053, pp. 92–100, 2003.
- [13] T. Campos de Almeida, "Desenvolvimento de asa morfica atuada por fios de NiTi com efeito de memoria de forma," Ph.D. dissertation, Instituto Tecnológico de Aeronáutica, 2016.
- [14] J. Mohd, M. Leary, A. Subic, and M. A. Gibson, "A review of shape memory alloy research , applications and opportunities," *Materials and Design*, vol. 56, pp. 1078–1113, 2014. [Online]. Available: <http://dx.doi.org/10.1016/j.matdes.2013.11.084>
- [15] H. Föll, "Twinning, Shear Deformation and Martensite Formation," in *Iron, Steel and Swords script*.
- [16] L. Robatto, M. Magalhaes, and V. Junqueira, "Sistema de asa flexível com dupla atuação de fios de liga com efeito de memória de forma Conteúdo," pp. 1–14, 2015.
- [17] D. A. Miller and D. C. Lagoudas, "Thermomechanical characterization of NiTiCu and NiTi SMA actuators : influence of plastic strains."
- [18] T. A. Weisshaar, "Morphing Aircraft Systems : Historical Perspectives and Future Challenges," vol. 50, no. 2, 2013.
- [19] T. G. Ivanko, R. C. Scott, M. H. Love, S. Zink, T. A. Weisshaar, I. Introduction, L. Martin, A. Engineer, A. Branch, S. A. Engineer, A. Branch, S. S. Engineer, and S. Engineer, "Wind Tunnel Testing," no. April, pp. 1–17, 2007.
- [20] V. Piccirillo, "Caracterização, dinâmica não-linear e modelagem de atuadores com memória de forma para aplicações em aeroservoelasticidade," Ph.D. dissertation, Instituto Tecnológico de Aeronáutica, 2012.